THE ASTROPHYSICAL JOURNAL, 342:493–515, 1989 July 1

X-RAY, ULTRAVIOLET, AND OPTICAL OBSERVATIONS OF THE INTERMEDIATE POLAR FO AQUARII (H2215−086)

L. CHIAPPETTI,[1] T BELLONI,[2,3] J.-M. BONNET-BIDAUD,[4] C. DEL GRATTA,[2] D. DE MARTINO,[5] L. MARASCHI,[2] M. MOUCHET,[6] K. MUKAI,[7] J. P. OSBORNE,[8] R. H. D. CORBET,[9] E. G. TANZI,[1] AND A. TREVES[2]

Received 1988 August 11; accepted 1988 December 13

ABSTRACT

An extensive set of quasi-simultaneous, multiwavelength observations of the intermediate polar FO Aqr (H2215−086) obtained in 1983–1985 with the *EXOSAT* and *IUE* satellites and from La Palma Observatory are presented. The rotational 21 minute period and sideband periods due to beating with the orbital modulation are observed in the optical band and in X-rays. In particular, it is noticeable that an unusual sideband frequency at $\Omega_{rot} + 2\Omega_{orb}$ is present in X-rays. Long-term variations are observed at UV and X-ray frequencies (including a variation of the shape of the X-ray light curve). The X-ray spectra (in the 0.1–10 keV band) are well described by a flat power law (photon index ~ 0.6). Variability of the spectrum with the rotation period is detected, which can be interpreted as modulation by an absorbing envelope. A possible improvement to the current orbital ephemeris, based on our photometric data, is also presented. The implications of the observations for the source models are briefly discussed.

Subject headings: stars: dwarf novae — stars: individual (FO Aqr) — ultraviolet: spectra — X-rays: binaries

I. INTRODUCTION

The *HEAO 1* X-ray source H2215−086 (Marshall *et al.* 1979) was located by means of the *Einstein Observatory* and identified with a cataclysmic variable (Patterson and Steiner 1983). The earliest photometric (Patterson and Steiner 1983) and spectroscopic (Shafter and Targan 1982) observations led to the discovery of two clear periodicities, a 4 hr "orbital" one and a 21 minute "rotational" one, and to the classification as an intermediate polar. Further spectroscopy was provided by Williams (1983), Mouchet (1983), and Penning (1985). A refined ephemeris for the rotational period was given by Sherrington, Jameson, and Bailey (1984). The rotational modulation was also detected in X-rays by Cook, Watson, and McHardy (1984). Arguments in favor of a spin-down were put forward by Pakull and Beuermann (1987) and confirmed by Shafter and Macry (1987, hereafter SM), who updated the rotational and orbital ephemerides. These ephemerides, where rotational phase 0 corresponds to the photometric maximum, and orbital phase 0 to the minimum, are used throughout this paper (see, however, below, § II*b*[i]).

The presence of an optical sideband period at 23 or 19 minutes is debated in Patterson and Steiner (1983; see also Pakull 1982 referenced therein) and Mouchet (1983), and is discussed by Warner (1986).

Here we report on *EXOSAT*, *IUE* and optical observations obtained as part of an extensive program of multiwavelength observations of magnetic cataclysmic variables. Part of our X-ray and UV data on H2215−086 were preliminarily presented by Maraschi *et al.* (1984), Mouchet and Bonnet-Bidaud (1984), Osborne *et al.* (1985*a*), and Chiappetti *et al.* (1988).

[1] Istituto di Fisica Cosmica del Consiglio Nazionale delle Ricerche, Milano, Italy.
[2] Dipartimento di Fisica dell'Università, Milano, Italy.
[3] Present address: Max-Planck-Institut für Extraterrestrische Physik, Garching, Federal Republic of Germany.
[4] Centre d'Etudes Nucléaires de Saclay, Gif-sur-Yvette, France.
[5] Osservatorio di Capodimonte, Napoli, Italy.
[6] Observatoire de Meudon, Meudon, France.
[7] Mullard Space Science Laboratory, Holmbury St. Mary, United Kingdom.
[8] Space Science Department, ESTEC, Noordwijk, The Netherlands.
[9] Department of Astrophysics, University of Oxford, United Kingdom.

II. OBSERVATIONS

H2215−086 was observed by us on two occasions (1983 October and 1985 October) in X-rays with the *EXOSAT* satellite, while same-day UV coverage was being provided by the *International Ultraviolet Explorer* (*IUE*). A third *IUE* observation (1984 July) was obtained quasi-simultaneously with optical spectroscopy from La Palma. *UBVRI* photometry was also secured on the same night and on two subsequent nights.

A journal of observations is given in Table 1. The analysis procedure and the results are described below separately for each instrument.

a) X-Rays

In both *EXOSAT* observations the source was observed with the medium-energy (ME) proportional counter array (Turner and Smith 1981) in an offset configuration, with one half of the experiment pointed at the target and the other half monitoring the background. Only data from the argon chambers (four chambers for each experiment half) are discussed here. In both observations the HER3 or HER4 mode was employed, i.e., one set of 128 channel spectra was collected every 10 s.

Data from the channel multiplier array (CMA) in focus of the low-energy (LE) telescopes (de Korte, Bleeker, and den Boggende 1981) are also available. In 1983 the two telescopes (LE1 and LE2) were used respectively with the 3000 Å Lexan and aluminum/parylene filters. No time-resolved measurements are possible in the soft X-ray band owing to the weakness of the source: the integrated count rates are reported in Table 2. In 1985 only the LE1 telescope was available, and it was used with the 3000 Å Lexan filter. The source was, however, not detected, and only an upper limit is reported in Table 2.

The ME background subtraction proved troublesome. No array swap was performed (the two halves were in the same

TABLE 1

JOURNAL OF OBSERVATIONS

A. *EXOSAT*

Detector Configuration	Epoch		Observer
ME half 2; HER3 detector identifier	1983 Oct 11	03:49–10:57	Osborne
LE1 + thin Lexan filter	1983 Oct 11	04:17–10:36	
LE2 + Al/parylene filter	1983 Oct 11	04:14–10:36	
ME half 2; HER4 detector identifier	1985 Oct 22/23	19:54–01:33	Chiappetti
LE1 + thin Lexan filter	1985 Oct 22/23	20:21–01:31	

B *IUE*

Camera and Image Number	Epoch[a]		Observer
SWP 21272	1983 Oct 11	16:00 (63)	Bonnet-Bidaud
SWP 21273	1983 Oct 11	18:01 (63)	
SWP 21274	1983 Oct 11	18:56 (42)	
SWP 21275	1983 Oct 11	21:10 (31)	
LWR 16967	1983 Oct 11	14:41 (63)	
LWP 2027	1983 Oct 11	17:12 (42)	
LWP 2028	1983 Oct 11	19:10 (42)	
LWP 2029	1983 Oct 11	20:43 (21)	
SWP 23511	1984 Jul 25	20:05 (50)	Treves
SWP 23512	1984 Jul 25	21:30 (50)	
SWP 23513	1984 Jul 25	22:54 (50)	
SWP 23514 (multiple exposure)	1984 Jul 26	00:36 (49)	
LWP 3872	1984 Jul 25	21:01 (20)	
LWP 3873	1984 Jul 25	22:36 (20)	
LWP 3874	1984 Jul 25	23:56 (20)	
SWP 26965	1985 Oct 22	15:02 (42)	Maraschi
SWP26966	1985 Oct 22	16:20 (42)	
SWP 26967	1985 Oct 22	17:38 (42)	
SWP 26968	1985 Oct 22	19:29 (42)	
LWP 6969	1985 Oct 22	15:50 (21)	
LWP 6970	1985 Oct 22	17:11 (21)	
LWP 6971	1985 Oct 22	18:29 (21)	
LWP 6972	1985 Oct 22	20:19 (21)	

C. LA PALMA

Detector configuration	Epoch		Observer
INT + IPCS + RGO spectrograph; 91 spectra (~100 s each)	1984 Jul 25/26	23:53–04:20	Corbet/Mukai
JKT + *UBVRI* photometer	1984 Jul 26	00:21–05:03	van der Klis
	1984 Jul 30	00:15–04:50	
	1984 Jul 31	00:30–04:10	

[a] In the case of *IUE* observations, the epoch given is the start time of the exposure, with its overall duration in minutes in parentheses. Multiple exposures have not been considered in the present work.

mechanical configuration during the slew and during the pointing period), therefore a reference background had to be obtained from the best parts of the slew maneuver data.

For the purpose of temporal analysis, light curves (see below) and time-resolved spectra were produced using the following background subtraction procedure: first the instantaneous background in the offset half (half 1) was subtracted from the measurement in the aligned half (half 2), and then the result was compensated for the intrinsic background difference of the two halves, by subtracting the difference between the above-mentioned reference background spectra (half 2 minus half 1).

For spectral fitting, where a higher statistical quality is required, phase-resolved spectra were produced (see Table 2 for phase intervals used), subtracting the background in the offset half (integrated over the whole observing period) and then compensating as above. The same procedure was used in the case of the average spectra (integrated over the whole observing period) used to derive the mean count rates reported in Table 2.

i) *Light Curves*

Background-subtracted light curves for both observations, in the pulse-height (PHA) channel range 6–40 (*ca.* 1–10 keV), are shown in Figure 1. The average count level in both years is substantially higher than the one reported for 1983 August by Cook, Watson, and McHardy (1984).

The 21 minute rotational periodicity is clearly visible. It is apparent from the light curves in separate energy bands (1–5 and 6–10 keV) that the modulation is larger at lower energies. The 1983 light curve is more erratic than that of 1985, and shows a slight rising trend over the observing period, again more evident at higher energies. In 1985 the source was in a lower state for part of the time (~23:15–00:30 UT), with weaker rotational modulation.

TABLE 2

SUMMARY OF X-RAY COUNT RATES

A. *EXOSAT* MEDIUM ENERGY

NOTES	EXPOSURE (s)	COUNT RATES (counts s^{-1} $half^{-1}$) 1–5 keV	6–10 keV	1–10 keV
1983 October 11				
Overall interval	24670	0.83 ± 0.04	1.04 ± 0.04	2.01 ± 0.05
High (phases 0.02–0.32)	6190	1.48 ± 0.06	1.19 ± 0.06	2.88 ± 0.09
Low (phases 0.42–0.92)	11220	0.60 ± 0.06	0.91 ± 0.06	1.63 ± 0.08
1985 October 22/23				
Overall interval	20220	0.90 ± 0.04	0.95 ± 0.04	2.06 ± 0.05
High (phases 0.04–0.54)	9720	1.14 ± 0.05	1.03 ± 0.06	2.48 ± 0.08
Low (phases 0.59–0.94)	5880	0.55 ± 0.06	0.71 ± 0.06	1.40 ± 0.09

B. *EXOSAT* LOW ENERGY

Notes	Exposure (s)	Net Counts	Corrected Count Rate (10^{-3} counts s^{-1})
1983 October 11; LE1 + Lexan			
Overall interval	18979	27.9 ± 7.0	2.35 ± 0.59
High	5600	22.1 ± 5.3	6.28 ± 1.50
Low	9639	5.6 ± 6.4	<3.40
1983 October 11; LE2 + Al/Parylene			
Overall interval	21866	24.8 ± 7.0	1.77 ± 0.50
High	6580	22.9 ± 5.5	5.43 ± 1.3
Low	10896	1.5 ± 3.6	<2.17
1985 October 22; LE1 + Lexan			
Overall interval	15904	−2.6 ± 4.3	<1.46
High	4394	−2.0 ± 2.0	<3.11
Low	9852	−1.0 ± 3.3	<2.02

NOTE.—The background subtraction for ME count rates is described in the text. The "high" and "low" phase intervals correspond to the flatter parts of the folded light curves in Fig. 3. In the case of the LE experiment, we give the net number of counts measured in an 11 × 11 pixel box (1 pixel = 4″) around the expected source position, after subtraction of the background as determined by an outer larger corona. The count rates (or 3 σ upper limits where applicable) have been corrected for dead time, point-spread function, background non-uniformity, and vignetting effects. To enable a direct comparison with ME count rates, data have also been accumulated in the same phase interval used in the ME case.

ii) *Temporal Analysis*

Periodograms were obtained using the method of Ferraz-Mello (1981) (used throughout this paper) and are shown in Figure 1 together with the X-ray light curves. A number of characteristic peaks are apparent in the power spectrum, namely, (1) a strong peak at the 21 minute rotational period (P_{rot}); (2) an ill-defined low-frequency excess (the width of which includes the orbital period; however, the limited length of the observations precludes any conclusion in the low-frequency domain); (3) two peaks at the two beat frequencies ($\Omega_{rot} + \Omega_{orb}$ and $\Omega_{rot} + 2\Omega_{orb}$, hereafter labeled as the S^+ and S^{++} *sidebands*); (4) the higher harmonics of P_{rot} (in the 1985 observation only).

A complete summary of the main periodicities found, together with their significance, is given in Table 3C. Similar results are obtained with a χ^2 folding search (not shown), which allows the estimate of the uncertainty on the periods of the order of 30 s. The following points are worth noticing.

The rotational period shows up very clearly and is consistent with the ephemeris of SM to within the width of our peaks. The fact that one can see the higher harmonics (up to perhaps the third one) only in 1985 is suggestive of a change in the shape of the light curve (which is actually confirmed by a folding analysis; see below).

We also find very clear evidence in X-rays for the two sidebands S^+ and S^{++}. The peaks are clearly distinct from and in excess above any feature induced by spectral window effects; in 1985 the S^+ peak appears sometimes as a shoulder in the main peak. There is generally a lack of power on the low-frequency side of P_{rot} (where one could expect the sidebands S^- and S^{--} at frequencies $\Omega_{rot} - \Omega_{orb}$ and $\Omega_{rot} - 2\Omega_{orb}$), except perhaps for some marginal evidence in 1985.

Concerning the energy dependence of the temporal variability, the rough subdivision in two energy bands only shows that any periodic modulation is stronger at lower energies. We performed the Fourier analysis simultaneously for all PHA channels and converted the height of the peaks in the power spectra to significances, according to the prescriptions in Ferraz-Mello

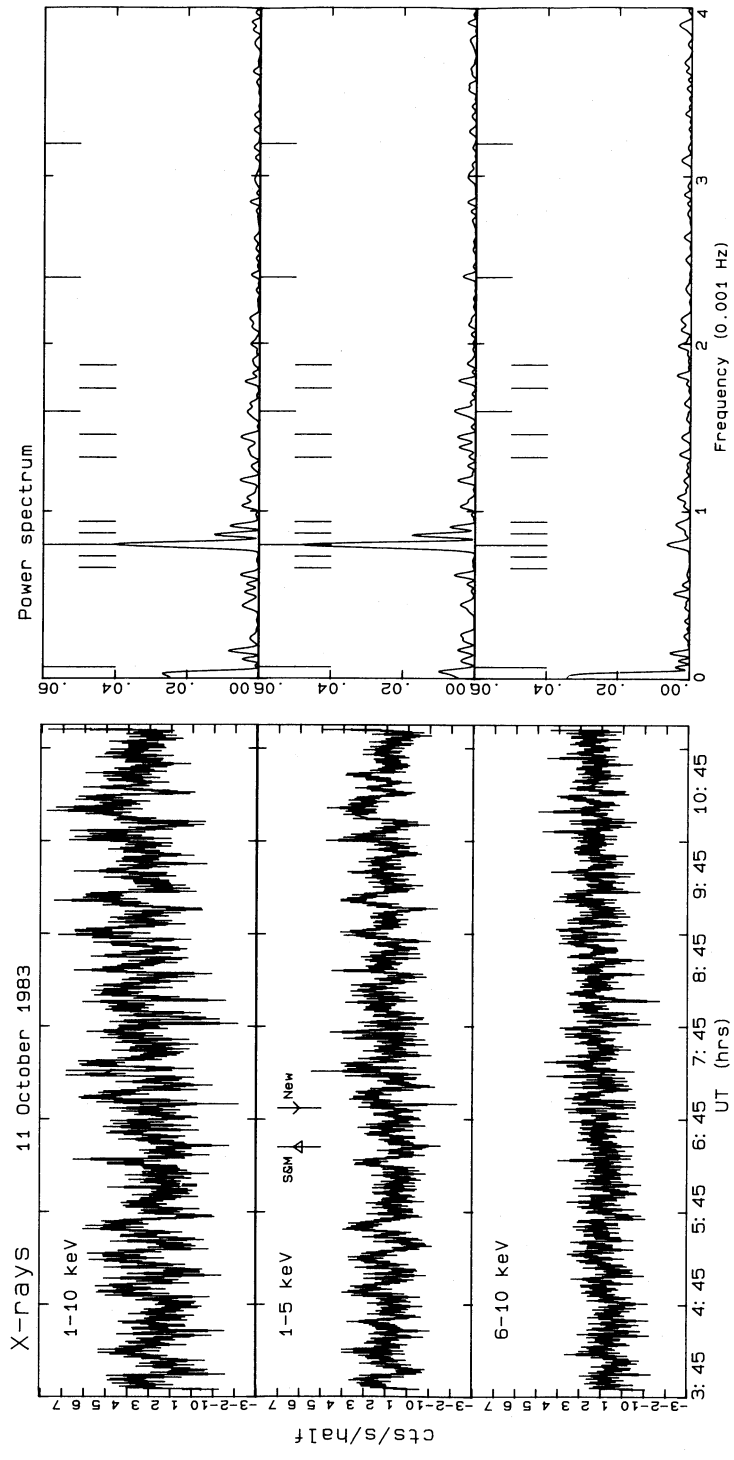

FIG. 1a

FIG. 1.—(*a*, *b*) X-ray light curves and periodograms. In the light curve frames two fiducial marks indicate orbital phase 0 according to SM (*up arrow*) and to the ephemeris derived in this paper (*down arrow*). Fiducial marks in the periodograms indicate (*from left to right*) the positions of the orbital frequency, the S^{--} and S^{-} sidebands, the rotational frequency, the S^{+} and S^{++} sidebands, the first harmonics of the sidebands and of the rotational frequency and (for 1985 alone) the higher harmonics of the rotational frequency (all according to SM ephemeris).

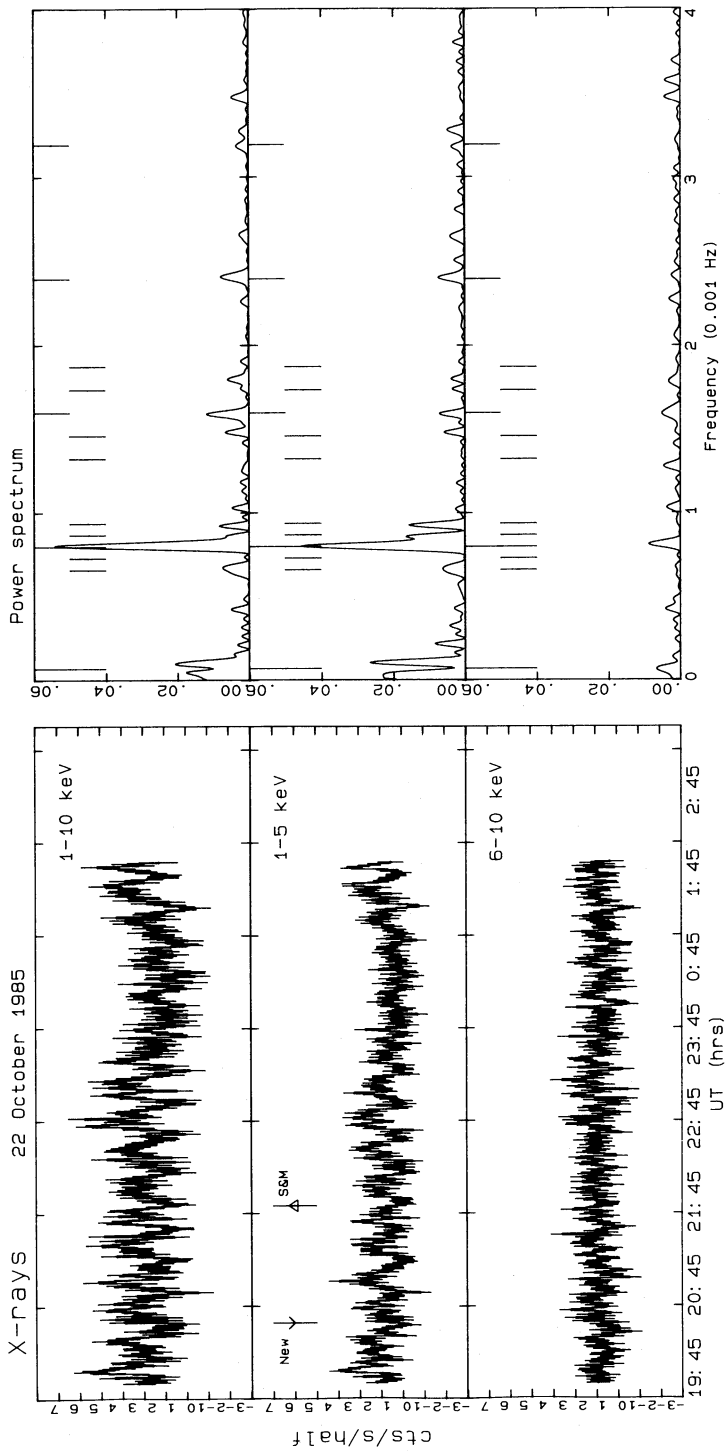

FIG. 1*b*

TABLE 3A

SUMMARY OF TEMPORAL ANALYSIS RESULTS: PERIODICITIES FOR PHOTOMETRIC OBSERVATIONS

Observation (1984)	*N* Bin	"Long" Period (14517 s = P_{orb})	Sidelobe S^{--} (1516.6 s)	Sidelobe S^{-} (1373.1 s)	P_{rot} (1254.5 s)	Sidelobe S^{+} (1154.7 s)	Sidelobe S^{++} (1069.6 s)
U band:							
Jul 26	62	15385 2×10^{-6}	1563 6×10^{-2}	1398 8×10^{-2}	1227 3×10^{-5}	1156[a]	1098[a]
Jul 30	206	22222 1×10^{-16}	1504 4×10^{-4}	1398[a]	1266 5×10^{-14}	1163[a]	...
Jul 31	179	10000 7×10^{-8}	1515 2×10^{-3}	...	1290 2×10^{-19}	1143 9×10^{-4}	...
Combined	458	14285[b] 8×10^{-7}	1538 1×10^{-5}	[c]	1274 4×10^{-29}	[c]	...
B band:							
Jul 26	62	14286 1×10^{-5}	1550 1×10^{-2}	1398[a]	1235 5×10^{-5}	1149[a]	1053[a]
Jul 30	206	20000 9×10^{-21}	1504 6×10^{-6}	1370 2×10^{-4}	1250 7×10^{-8}	1163 4×10^{-3}	...
Jul 31	179	10000 9×10^{-14}	1515 1×10^{-2}	...	1290 3×10^{-15}	1136 7×10^{-3}	...
Combined	458	14285[b] 2×10^{-15}	1515 1×10^{-6}	1370 2×10^{-8}	1274 1×10^{-18}	[c]	...
V band:							
Jul 26	62	14286 3×10^{-5}	1562 1×10^{-2}	1409[a]	1235 3×10^{-4}	1143[a]	1053[a]
Jul 30	206	20000 1×10^{-21}	1504 4×10^{-5}	1370 6×10^{-4}	1250 4×10^{-8}	1163 7×10^{-3}	...
Jul 31	179	10000 2×10^{-15}	1515 5×10^{-2}	...	1290 4×10^{-14}	1130 8×10^{-3}	...
Combined	458	12500[b] 1×10^{-17}	1515 4×10^{-7}	1370 1×10^{-7}	1274 3×10^{-17}	[c]	...
R band:							
Jul 26	62	15385 2×10^{-4}	1575 7×10^{-3}	1428[a]	1235 6×10^{-4}	1156[a]	...
Jul 30	206	20000 7×10^{-23}	1515 7×10^{-5}	1360 2×10^{-3}	1250 2×10^{-8}	1183 5×10^{-3}	...
Jul 31	179	10000 5×10^{-16}	1515 6×10^{-2}	...	1290 6×10^{-14}	1136 2×10^{-2}	...
Combined	458	14285[b] 9×10^{-21}	1515 4×10^{-6}	1370 1×10^{-6}	1274 5×10^{-16}	[c]	...
I band:							
Jul 26	62	18181 3×10^{-4}	1587 1×10^{-2}	...	1242 2×10^{-2}	...	...
Jul 30	206	20000 9×10^{-21}	1504 4×10^{-4}	1408 5×10^{-3}	1242 2×10^{-7}	1183 2×10^{-3}	...
Jul 31	179	10000 2×10^{-15}	1538 1×10^{-2}	...	1299 3×10^{-12}	1136 3×10^{-2}	...
Combined	458	14285[b] 6×10^{-21}	1515 3×10^{-4}	1370 3×10^{-5}	1274 9×10^{-12}	[c]	...

TABLE 3B

SUMMARY OF TEMPORAL ANALYSIS RESULTS: PERIODICITIES FOR SPECTROSCOPIC OBSERVATIONS

Observation[d]	*N* Bin	"Long" Period (14517 s = P_{orb}; 7258 s = $P_{orb}/2$)	Sidelobe S^{--} (1516.6 s)	Sidelobe S^{-} (1373.1 s)	P_{rot} (1254.5 s)	Sidelobe S^{+} (1154.7 s)	Sidelobe S^{++} (1069.6 s)
EW:							
He II	90	8000 2×10^{-6}	...	1351 7×10^{-3}	1235 6×10^{-2}	1143 6×10^{-2}	...
Hβ	90	7407 3×10^{-6}	...	1380 4×10^{-3}	1242 4×10^{-2}	1124 2×10^{-2}	...
Hγ	90	7143 1×10^{-5}	...	1370 6×10^{-4}	1227 0.2	1117 7×10^{-2}	...
Velocity:							
He II	91	15385 4×10^{-9}	...	1429 1×10^{-2}	1242 1×10^{-3}	...	...
Hβ	91	9524 3×10^{-5}	...	1351 2×10^{-4}	...	1190 2×10^{-2}	...
Hγ	91	8333 4×10^{-4}	...	1379 4×10^{-3}	...	1198 3×10^{-3}	...
Hδ	87	8000 6×10^{-5}	...	1379 3×10^{-2}	...	1212 7×10^{-3}	...

TABLE 3C

SUMMARY OF TEMPORAL ANALYSIS RESULTS: PERIODICITY FOR X-RAY OBSERVATIONS

Observation	*N* Bin	"Long" Period (14517 s = P_{orb})	Sidelobe S^{--} (1516.6 s)	Sidelobe S^{-} (1373.1 s)	P_{rot} (1254.5 s)	Sidelobe S^{+} (1154.7 s)	Sidelobe S^{++} (1069.6 s)
1983:							
1–10 keV	2467	33333 5×10^{-15}	...	...	1250 2×10^{-22}	1163 2×10^{-7}	1099 5×10^{-5}
1–5 keV	2467	22222 6×10^{-6}	...	...	1250 8×10^{-27}	1169 5×10^{-10}	1105 2×10^{-4}
6–10 keV	2467	Undefined 6×10^{-19}	...	...	1242 4×10^{-4}	[c]	1087 7×10^{-3}
1985:							
1–10 keV[d]	2022	10000 9×10^{-10}	1481 6×10^{-4}	[c]	1242 2×10^{-24}	1169[a]	1087 3×10^{-4}
1–5 keV[d]	2022	9523 2×10^{-12}	1504 2×10^{-3}	...	1250 1×10^{-20}	1169 6×10^{-8}	1081 1×10^{-7}
6–10 keV[d]	2022	15383 1×10^{-3}	...	...	1235 1×10^{-4}	...	...

TABLE 3D

SUMMARY OF TEMPORAL ANALYSIS RESULTS: HIGHER HARMONICS

I. SPECTROSCOPIC OBSERVATIONS

Observation	$S^-/2$ (687 s)		$P_{rot}/2$ (627 s)	
EW:				
He II	671	5×10^{-2}	...	
Hβ	667	6×10^{-3}	...	
Hγ	676	4×10^{-3}	...	
Velocity:				
He II	...		613	8×10^{-2}
Hβ	660	6×10^{-3}	...	
Hγ	660	7×10^{-3}	...	
Hδ	667	1×10^{-2}	...	

II. X-RAY OBSERVATION

Observation (1985)	$S^-/2$ (687 s)		$P_{rot}/2$ (627 s)		$S^+/2$ (577 s)		$P_{rot}/3$ (418 s)		$P_{rot}/4$ (314 s)	
1–10 keV	676	1×10^{-3}	629	7×10^{-6}	557	2×10^{-3}	416	4×10^{-4}	315	4×10^{-2}
1–5 keV	676	3×10^{-3}	629	8×10^{-4}	555	2×10^{-2}	417	6×10^{-4}	305	9×10^{-3}
6–10 keV		...	629	5×10^{-3}		...		...		...

NOTES TO TABLES 3A–3D

NOTE.—For each component, two adjacent columns indicate respectively the measured period value in seconds (position of the peak in the power spectrum) and the chance probability according to Ferraz-Mello (1981). The reference value of each period is indicated in parentheses below each column heading.

[a] The significance of this peak cannot be measured directly; however, the peak is apparent once the component at P_{rot} has been subtracted.

[b] In the case of the combination of the three nights of photometry, the peak closest to P_{orb} is indicated in this column, even if it is not the highest peak at the low-frequency end of the power spectrum.

[c] The peak cannot be easily resolved, because of the complex shape of the spectral window.

[d] Information on higher harmonics is available in Table 3D.

(1981). Figure 2 is a map of the significance contours in the energy-frequency plane. Of course, this way the statistics in each PHA channel may be quite low. Compare also Figure 3 of Chiappetti *et al.* (1988), where folded light curves for individual PHA channels are presented.

Modulation at P_{rot} is clearly apparent at all energies between 2 and 6 keV, with a sharp cutoff above the latter energy. Modulation at the high-frequency sidebands appears curiously concentrated in some very limited energy bands.

In order to examine the shape and phasing of the X-ray modulation, we folded the X-ray light curves with the optical rotational period known from the ephemeris of SM; the result is shown in Figure 3.

One can clearly see a change in shape, independent of the binning used for folding, between the two epochs; one aspect of this change can be quantified by a measurement of the pulsed fraction, which is reported in Table 4. It is apparent that the modulation is higher than expected for a sinusoid, that the maximum modulation is apparent in the lower energy band, and that the pulsed fraction is larger in the 1985 light curve.

The 1983 light curve appears quasi-sinusoidal, with the exception of the two spikes at phases 0 and 0.75. The 1985 light curve instead shows a secondary minimum at phase 0.25, and a narrower principal minimum. The two curves are well aligned on the sharp spike at phase 0.0 (optical phase 0.0 corresponds to the times of maxima). The leading edge of this spike appears to be a real feature, which is present very clearly in both years, independent of the binning used for the folding.

In order to study a possible phase shift, we generated, for each year, a template light curve, duplicating the cycles of the respective folded light curve. We then correlated the template with the data, repeatedly applying a shift of 1 phase bin. We then plotted the correlation coefficient against the shift and determined the maxima of the correlation with a parabolic fit to the peaks. This gives nominally a delay of 148.6 ± 72.6 s for 1983 and 181.8 ± 90.7 s for 1985 (the errors quoted are 1 σ), which leads to the conclusion that the data are consistent with the two X-ray light curves being in phase with each other, and with the optical ephemeris of SM.

iii) *Spectral Analysis*

In order to study the phase dependence of the spectra, we divided each X-ray observation into 2 phase intervals (see Table 2), corresponding to the high and low parts of the folded light curve, and accumulated a complete ME spectrum in each interval (labeled as "high spectrum" and "low spectrum"). We tried to use intervals where the count rate is reasonably constant (the flatter parts of the light curve), therefore the intervals have unequal length. These phase-resolved spectra were submitted to a standard χ^2 fitting procedure with simple spectral forms in the PHA channel range 12–40. The data were rebinned in order to achieve a signal-to-noise ratio of at least 3 σ in each bin; this way we were forced to reject the lowest channels. The results of the fits are summarized in Table 5. The reconstructed spectra are shown in Figure 4.

Blackbody and power-law spectral forms give fits of comparable quality (see also Fig. 4), while thermal bremsstrahlung generally shows higher χ^2 values and indicates a poorly constrained high temperature (not uncommon for hard spectra). The relatively poor quality of our data (particularly of our low

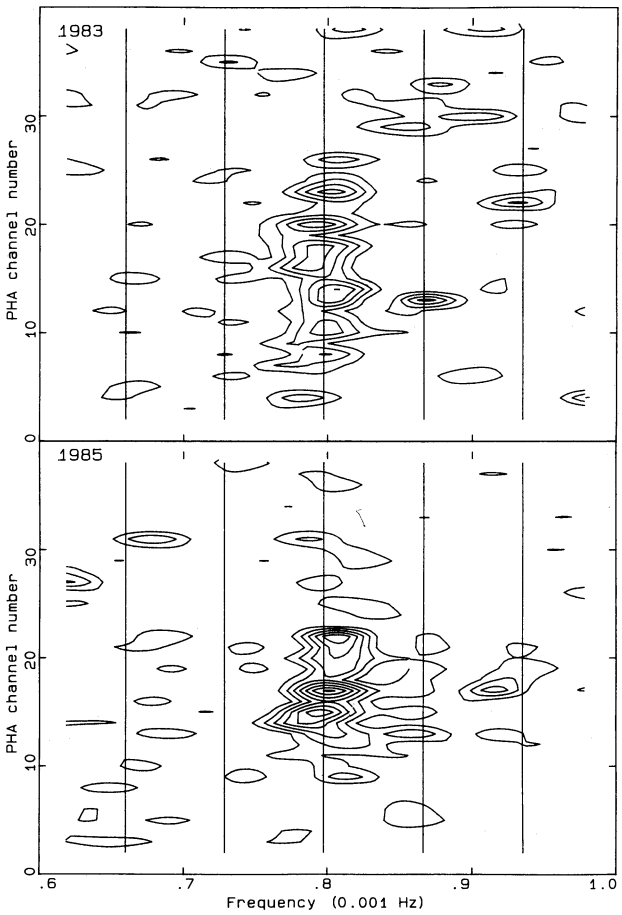

FIG. 2.—Periodogram for individual channels. The figure reports the result of a simultaneous periodogram generation for all PHA channels (in the range 1–40). The power has been converted into significances according to Ferraz-Mello (1981): the contours correspond to chance probabilities of 10^{-1}, 10^{-2}, 10^{-3}, 10^{-4}, 10^{-5}, 10^{-6}, and 10^{-7}. The vertical lines mark the positions of the rotational frequency and of the four sidebands. Note that the PHA channel ranges used in both Fig. 1 and Fig. 3 are respectively 6–21 (1–5 keV), 24–40 (6–10 keV) and 6–40 (1–10 keV).

spectra) precludes the use of more complex models (e.g., multi-temperature bremsstrahlung components as in Rosen, Mason, and Córdova 1988).

In both our 1983 and our 1985 observations the fits to the high spectra (ME data alone) indicate a loosely determined hydrogen column density of the order of 10^{22} cm^{-2}, but often consistent with zero (particularly in the blackbody case; see the confidence contours in Fig. 4).

A much higher column density ($\geq 10^{23}$ cm^{-2}) is instead systematically required by the low spectra. Although quite broad, the 90% confidence level contours are disjoint from those pertaining to the high spectra.

In the case of the 1983 high spectrum it is possible to fit the LE + filter count rates simultaneously with the ME data. The results are also given in Table 5 (and in Fig. 4*c*) and show some remarkable differences from the fits of the ME data alone. These include the following: (1) for any spectral form the hydrogen column density is forced to much lower values; (2) the thermal bremsstrahlung and blackbody spectral forms are ruled out; and (3) a power law is able to fit the LE and ME data quite well, with an extremely flat spectrum.

It is unfortunately not possible to use the LE data for the 1983 low phase interval, or for the 1985 observation. The upper limits are quite relaxed, and therefore consistent with the "ME only" best fits, but are unable to further constrain the spectral fit parameters. While the explanation of the low states as due to increased absorption alone remains tenable, it is not possible to confirm whether, in the high states, the column density in 1985 is higher than in 1983, as suggested by the disappearance of the source in the LE band, and also by the turnover in the lowest ME channels.

A final point concerns the presence of Fe lines, which appear rather common in other objects of the class (GK Per; 3A 0729+103; H2252−035; EX Hya; see references in discussion below). Some excess at 6–7 keV is apparent in our data (see in particular the count spectra in Fig. 4). Inspection of the residuals shows excesses of similar extent at other energies too, which are possibly due to imperfect background subtraction. We attempted to include a line in the fits, and the results are not discouraging. In all cases except the 1985 low spectrum there is some improvement in the χ^2. In particular, in the case of the 1983 LE + ME data (high spectrum) the best-fit photon index is $\sim$0.6 (i.e., slightly steeper than the one obtained without a line in the model), and the column density is $\sim 2 \times 10^{20}$ cm^{-2}, which leads also to an improved agreement between model and data in the LE range. However the uncertainty in the background evaluation prevents a meaningful determination of the line parameters and of the associated errors.

b) Optical

i) *Photometry*

Photometry in the *UBVRI* bands was obtained with the Jacobus Kapteyn Telescope (JKT) at La Palma during the night 1984 July 25–26 (simultaneously with our spectroscopic observations) and on two further nights (1984 July 29–30 and 30–31). The passbands used in the photometry duplicate the *UBV* system of Johnson and the *RI* system of Kron and Cousins (Bessell 1979). Individual integrations in each filter were 8 s long, and the filters were cycled in the sequence *IRVBU–UBVRI*.

We are also aware of a photometric measurement, quasi-simultaneous with our 1983 October 11 observation, which gave *B*-magnitudes of 12.83 at 6:55 UT and 13.43 at 8:08 UT (C. Hill and P. Henry 1983, private communication).

The optical light curves are shown in Figure 5. The source was at a comparable flux level in all bands during the three nights. All light curves show a clear rotational modulation, and a broad dip which could roughly be ascribed to the orbital modulation.

The five-band photometric data have been analyzed with Fourier techniques for the three nights separately, and joined together. The corresponding periodograms are shown in Figure 5. The data of the first night are quite sparse, while the subsequent two nights, and particularly the third, are of better quality. The periods of the peaks in the power spectra and their significances are reported in Table 3.

The height of the peak at the rotational frequency is always much higher in the *U* band, decreases abruptly going to the *B* band and then more gradually going to longer wavelengths (in the first night the rotational peaks in the *R* and *I* bands, although present, are comparable to the noise features). The height of the "long period" peak (which includes the orbital period) generally shows the opposite behavior.

We have also tried to subtract sinusoidal components

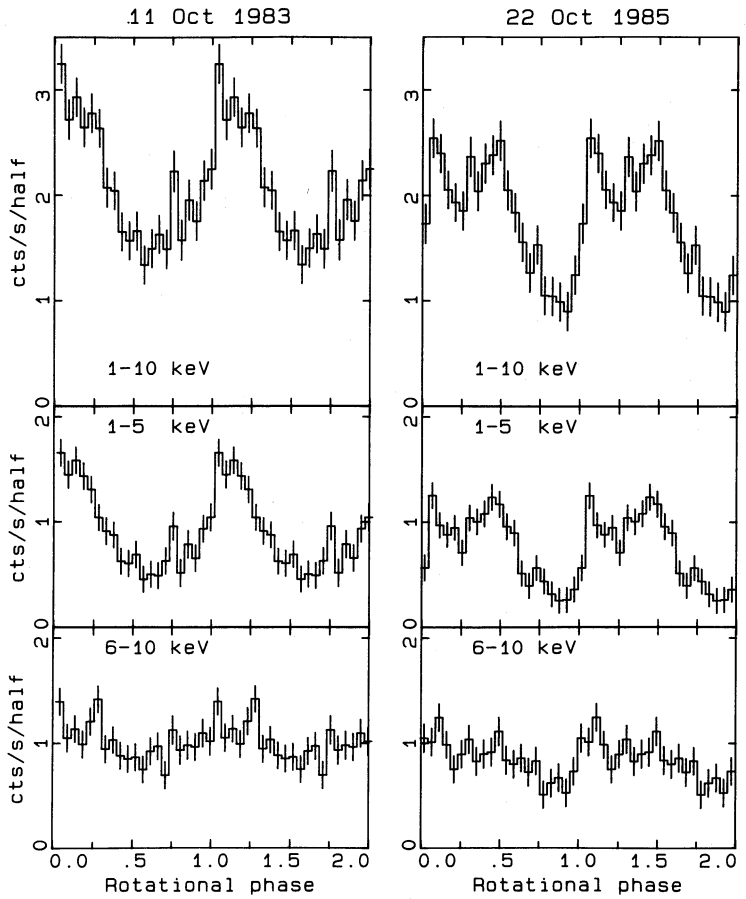

FIG. 3.—X-ray light curves in different energy bands, folded according to the (rotational) ephemeris of SM

TABLE 4

SUMMARY OF TEMPORAL ANALYSIS RESULTS: PULSED FRACTIONS

	From Folded Light Curve		From Sinusoidal Fit			
Band	Excursion	Pulsed Fraction	Excursion	Pulsed Fraction	Mean a_1	Amplitude a_2
X-Ray Observations, 1983 October, P_{rot}						
1–10 keV ...	0.59	0.36	0.49	0.32	2.08	0.67
1–5 keV	0.73	0.50	0.67	0.51	0.91	0.46
6–10 keV ...	0.51	0.31	0.28	0.16	1.01	0.17
X-Ray Observations, 1985 October, P_{rot}						
1–10 keV ...	0.65	0.50	0.51	0.34	1.78	0.61
1–5 keV	0.80	0.67	0.67	0.51	0.75	0.38
6–10 keV ...	0.59	0.40	0.32	0.19	0.85	0.16
Photometric Observations, 1984 July, P_{rot}						
U	0.34	0.19	0.31	0.18	4.30	0.78
B	0.26	0.15	0.24	0.14	2.64	0.36
V	0.22	0.13	0.20	0.11	1.55	0.17
R	0.20	0.11	0.17	0.09	0.94	0.09
I	0.24	0.12	0.16	0.09	0.53	0.04
Photometric Observations, 1984 July, P_{orb}						
U	0.32	0.23	0.23	0.13	4.24	0.61
B	0.42	0.30	0.27	0.16	2.58	0.42
V	0.41	0.29	0.32	0.19	1.52	0.24
R	0.40	0.28	0.36	0.22	0.92	0.14
I	0.39	0.25	0.35	0.21	0.53	0.11

NOTE.—The excursion is defined as the ratio (max − min)/max, while the pulsed fraction is the ratio of the area under the pulsed part of the light curve (i.e., above the minimum) to the total area under the light curve. In the case of a sinusoid $a_1 + a_2 \sin x$, of mean a_1 and amplitude a_2, the excursion is $2a_2/(a_1 + a_2)$ and the pulsed fraction is a_2/a_1. The units for a_1 and a_2 are counts s^{-1} $half^{-1}$ for the X-ray observations, and 10^{-14} ergs cm^{-2} s^{-1} $Å^{-1}$ for the optical observations.

TABLE 5

RESULTS OF SPECTRAL FITS

PARAMETER	1983 OCTOBER 11 High Phase	1983 OCTOBER 11 Low Phase	1985 OCTOBER 22 High Phase	1985 OCTOBER 22 Low Phase
Medium-Energy Data Only				
Degrees of freedom	21	14	19	11
Power law:				
Column density[a]	0.00 0.15 0.54	0.34 1.05 2.23	0.29 0.62 1.12	0.76 2.00 3.00
Photon index	0.19 0.54 1.00	−.10 0.48 1.35	0.55 0.98 1.50	0.27 1.35 2.27
2–10 keV flux[c]	4.45 4.75 4.99	2.84 3.08 3.25	3.95 4.17 4.39	2.27 2.52 2.80
χ^2	31.4	23.6	21.5	14.3
Blackbody:				
Column density[a]	0.00 0.00 0.15	0.13 0.60 1.50	0.00 0.19 0.31	0.21 1.00 2.29
kT (keV)	2.36 2.70 3.15	2.41 3.40 5.20	2.07 2.48 3.06	1.73 2.50 4.13
2–10 keV flux[c]	4.34 4.59 4.80	2.88 3.08 3.27	3.91 4.20 4.46	2.28 2.53 2.80
χ^2	28.6	21.5	18.8	13.4
Thermal bremsstrahlung:				
Column density[a]	0.63 0.86 1.06	1.68 2.20 2.90	0.80 1.00 1.24	1.48 2.10 3.30
kT (keV)	>37	>19	>25	>11
2–10 keV flux[c]	4.06 4.18 4.24	2.67 2.80 2.92	3.84 3.98 4.06	2.29 2.49 2.59
χ^2	47.3	29.1	25.0	14.4
Medium Energy plus Low Energy				
Degrees of freedom	23	...	...	...
Power law:				
Column density[b]	0.00 0.04 0.80	... ...	... ...	... ...
Photon index	0.19 0.31 0.56	... ...	... ...	... ...
2–10 keV flux[c]	4.62 4.83 4.92	... ...	... ...	... ...
1–2 keV flux[d]	2.12 2.28 2.95	... ...	... ...	... ...
0.5–1 keV flux[e]	6.21 6.95 8.88	... ...	... ...	... ...
χ^2	33.9	...	...	...
Blackbody:				
Column density[b]	0.00 0.00 1.45	... ...	... ...	... ...
kT (keV)	2.34 2.70 3.06	... ...	... ...	... ...
2–10 keV flux[c]	4.32 4.58 4.76	... ...	... ...	... ...
1–2 keV flux[d]	1.03 1.17 1.33	... ...	... ...	... ...
0.5–1 keV flux[e]	0.96 1.71 1.99	... ...	... ...	... ...
χ^2	50.3	...	...	...
Thermal bremsstrahlung:				
Column density[b]	3.04 4.00 5.53	... ...	... ...	... ...
kT (keV)	>83	... ...	... ...	... ...
2–10 keV flux[c]	3.70 3.80 4.00	... ...	... ...	... ...
1–2 keV flux[d]	5.20 5.60 6.00	... ...	... ...	... ...
0.5–1 keV flux[e]	5.78 9.45 11.3	... ...	... ...	... ...
χ^2	150	...	...	...

NOTE.—For each spectral fit parameter we give the best-fit value, bracketed by the extrema of the 90% confidence range. The fluxes given are at the source (the Morrison and McCammon 1983 cross sections have been used).

[a] The equivalent hydrogen column density is in units of 10^{23} atoms cm^{-2} for the ME fits.

[b] The equivalent hydrogen column density is in units of 10^{21} atoms cm^{-2} for the ME + LE fits.

[c] Flux in units of 10^{-11} ergs cm^{-2} s^{-1} for the 2–10 keV range.

[d] Flux in units of 10^{-12} ergs cm^{-2} s^{-1} for the 1–2 keV range.

[e] Flux in units of 10^{-13} ergs cm^{-2} s^{-1} for the 0.5–1 keV range.

(Ferraz-Mello 1981) and inspected the resulting light curves. Generally one can remove both periodicities/trends (i.e., the rotational modulation and the "orbital" dip clearly present in all light curves) quite well, but a residual variability is apparent, generally stronger in the *U* band. This is particularly evident in the third night. It looks as if there is a residual, low-level flaring, which occurs preferentially at the rotational maxima (a different case is a single "red" flare in the first night, which is highest in the *R* and *I* bands).

In Table 3 we give the significance of the sideband peaks closest to the expected sideband frequency. We also examined this by subtracting the main rotational periodicity from the light curves. On the first night sidebands are virtually absent, except perhaps on the low-frequency side in the *U* band. On the second night, however, they are present on both sides of the rotational frequency, and on the third a sideband can be seen on the high-frequency side. The effect is always small, at comparable intensities in all bands, or decreasing from the *U* to the *I* band. In the third night, however, a large peak at 1200 s (intermediate between the rotational peak and the usual high-frequency sideband) emerges in the *U* band only.

The examination of the power spectra for the combination of the three nights is made difficult by the complex shape of the spectral window. Some evidence for the orbital modulation is

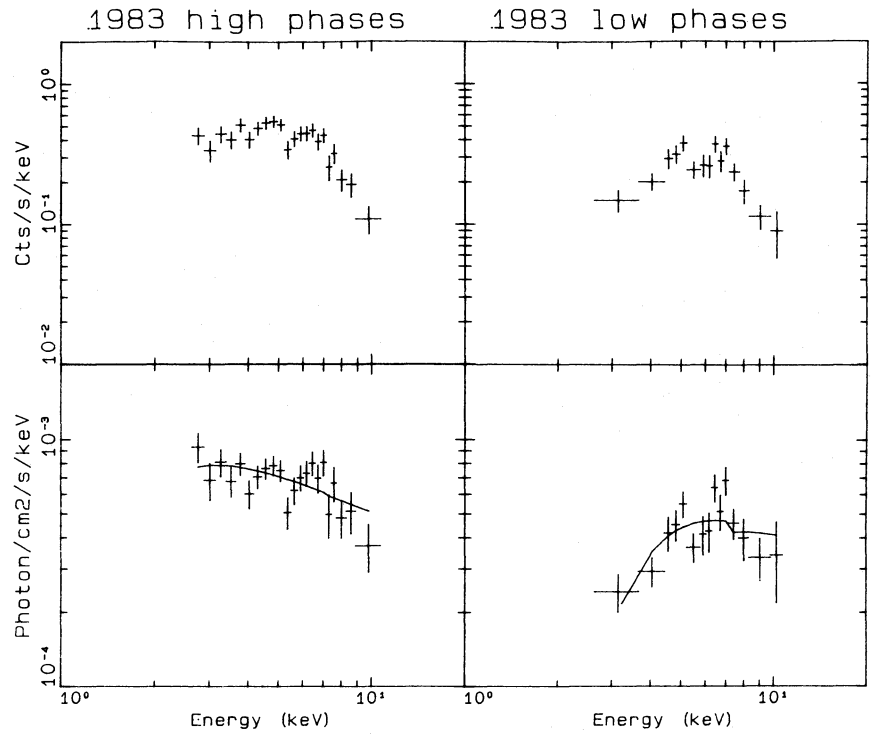

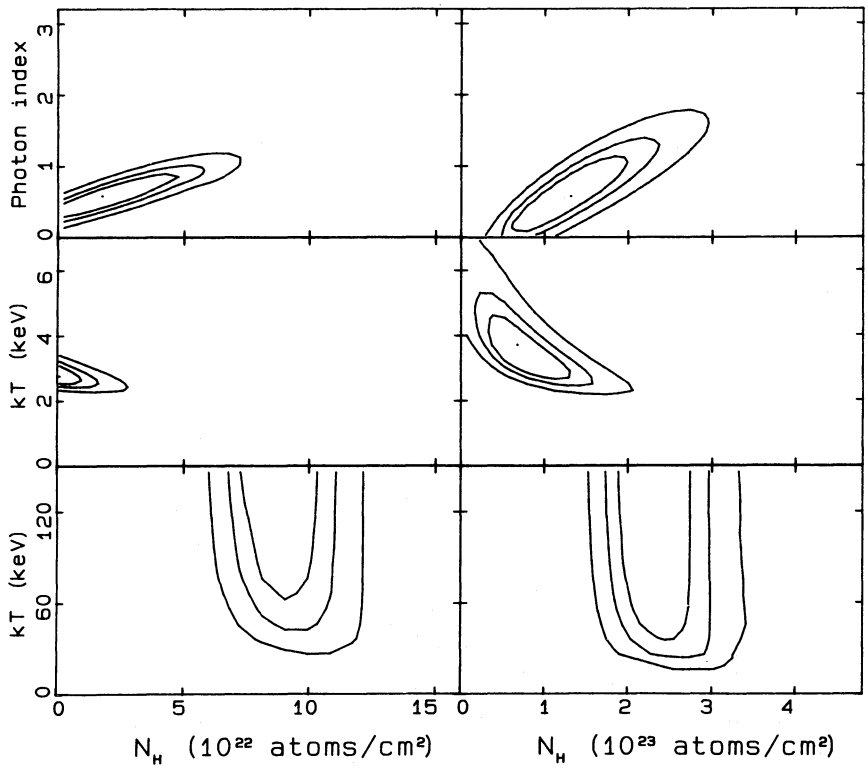

FIG. 4a

FIG. 4.—X-ray spectra. (*a*) 1983 ME data (high and low phase intervals); (*b*) 1985 ME data (high and low phase intervals); (*c*) 1983 ME and LE data (high phase interval only). The top panel spectrum shows the raw counts, while the lower panel contains the deconvoluted photon spectrum, together with the best-fit power law. The bottom panels show the 68%, 90%, and 99% confidence contours, respectively, for the power-law, blackbody, and thermal bremsstrahlung models (*top to bottom*). Note the different N_H scales used respectively for the low phases, the high phases, and the LE + ME data.

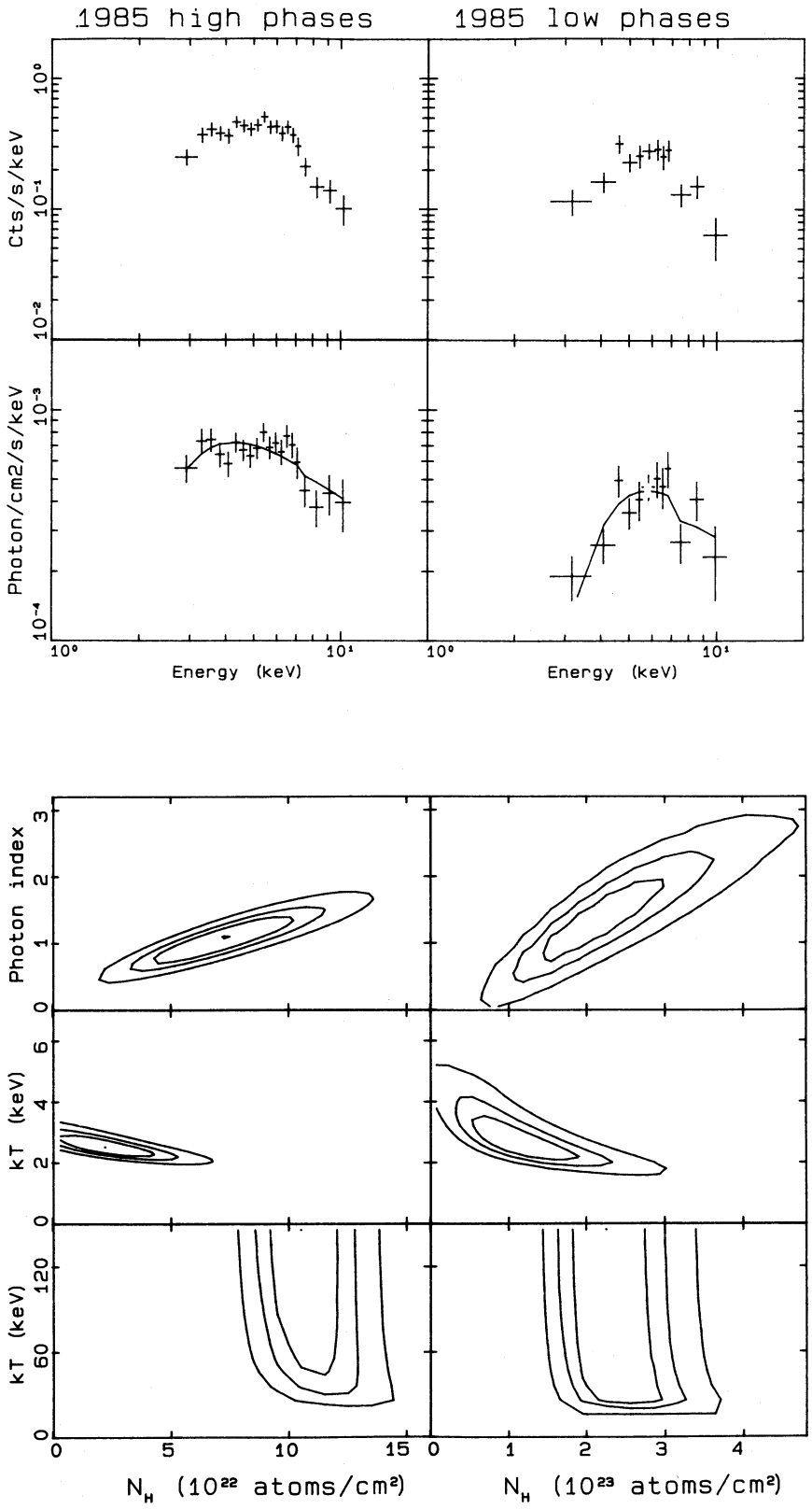

FIG. 4*b*

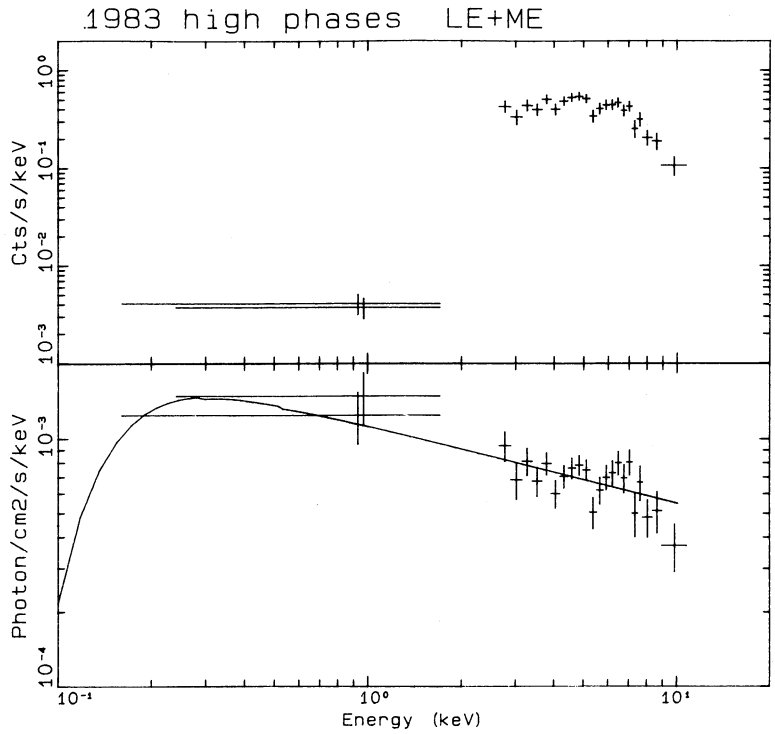

FIG. 4*c*

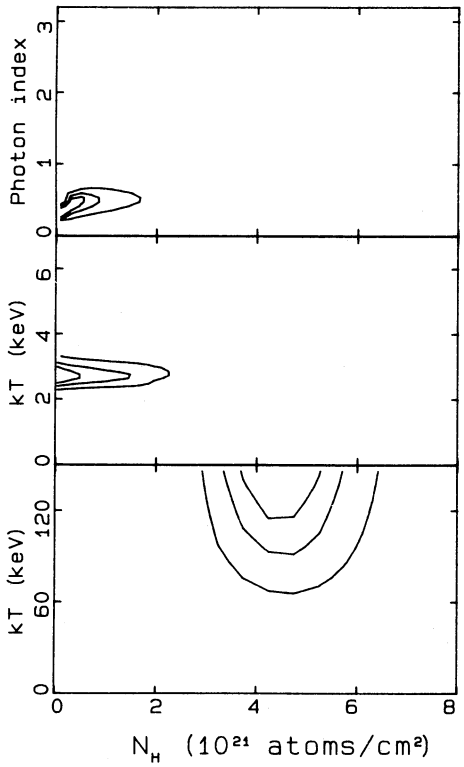

FIG. 4*c*—*Continued*

apparent at low frequencies. Possibly also some independent evidence for the S^- and particularly S^{--} sidebands is present.

The light curves folded according to SM at the rotational and orbital period are shown in Figures 6*a* and 6*b*, respectively. The shape of the rotational modulation appears sinusoidal, and exactly in phase with the SM ephemeris. In constrast, the orbital modulation is only roughly sinusoidal, and a square-shaped minimum occurs around phase 0.7 (instead of phase 0.0 as expected; see also Fig. 5*a*).

We further investigated the orbital phasing issue, considering that the observation by Berriman *et al.* (1986), used by SM, is only 2 weeks later than ours. It is apparent from Figure 1 of Berriman *et al.* that the light curve has a complex shape and it is difficult to determine the minimum. Examining the $O-C$ values reported by SM (their Table 2 and Fig. 2), one notices that the two points closer to our observation are the ones with the largest $O-C$ values, and with the largest difference among themselves! We have therefore computed a new orbital ephemeris, using all the *photometric* points in SM, plus the two minima on July 30 and 31 (timings are HJD 2,445,911.578 and HJD 2,445,912.596). We have excluded spectroscopic points, since there seem to be discrepancies between orbital solutions based on spectroscopy and photometry (M. Mateo 1988, private communication by P. Szkody). Our calculation gives a 4.85 hr period, with minimum at

$$\text{HJD } 2{,}445{,}761.6466(20) + 0.2020599(10)E \ .$$

The rms $O-C$ is 0.027, which is smaller than the value of 0.07 we get repeating the calculation for the data of SM (we have done this as a cross-check of the procedure, obtaining the same results as SM). It can be noted that 4.85 hr is the 1 day alias of 4.03 hr (Shafter and Targan 1982 had a similar situation).

The use of the new period instead of the one by SM does not affect any of our results concerning the sideband frequencies, since the width of the peaks in our periodograms is consistent with both cases.

Considering the pulsed fractions reported in Table 4, one may notice that the rotational light curve deviates more from a sinusoidal shape in the *R* and *I* bands, while the opposite is true for the orbital light curve (if instead of SM one uses our

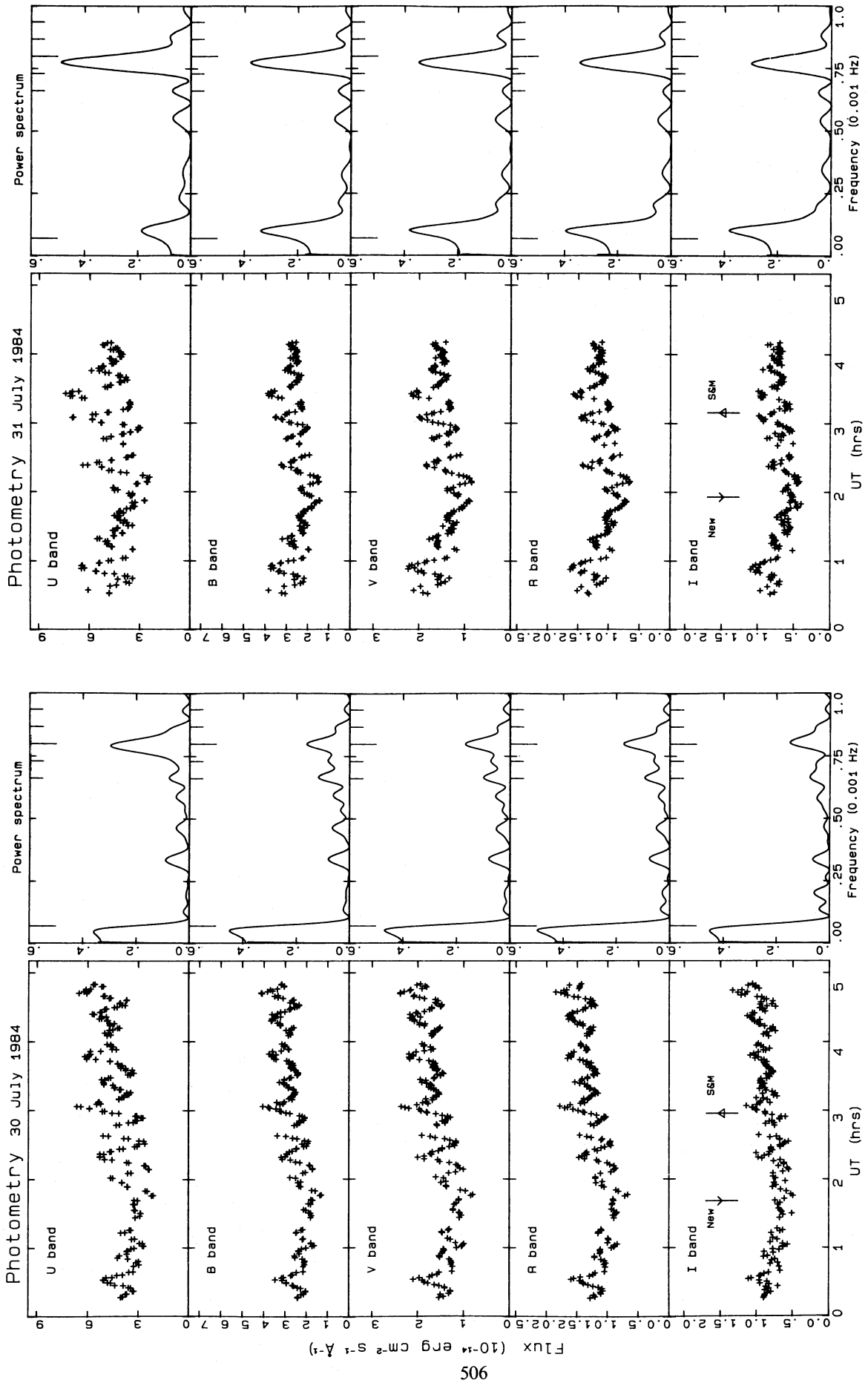

FIG. 5a

FIG. 5.—Optical light curves and related periodograms. The five band photometry data of the last two nights are shown, together with the corresponding periodogram (*a*). Additionally, the periodogram for the combination of all three nights of data is shown for each band (*b*). Fiducial marks in the periodograms indicate the positions of the orbital frequency, of the rotational frequency, and of the four sidebands. In the light curves the time of orbital phase 0 (according to SM and to the ephemeris derived in this paper) are marked with the same symbols used in Fig. 1.

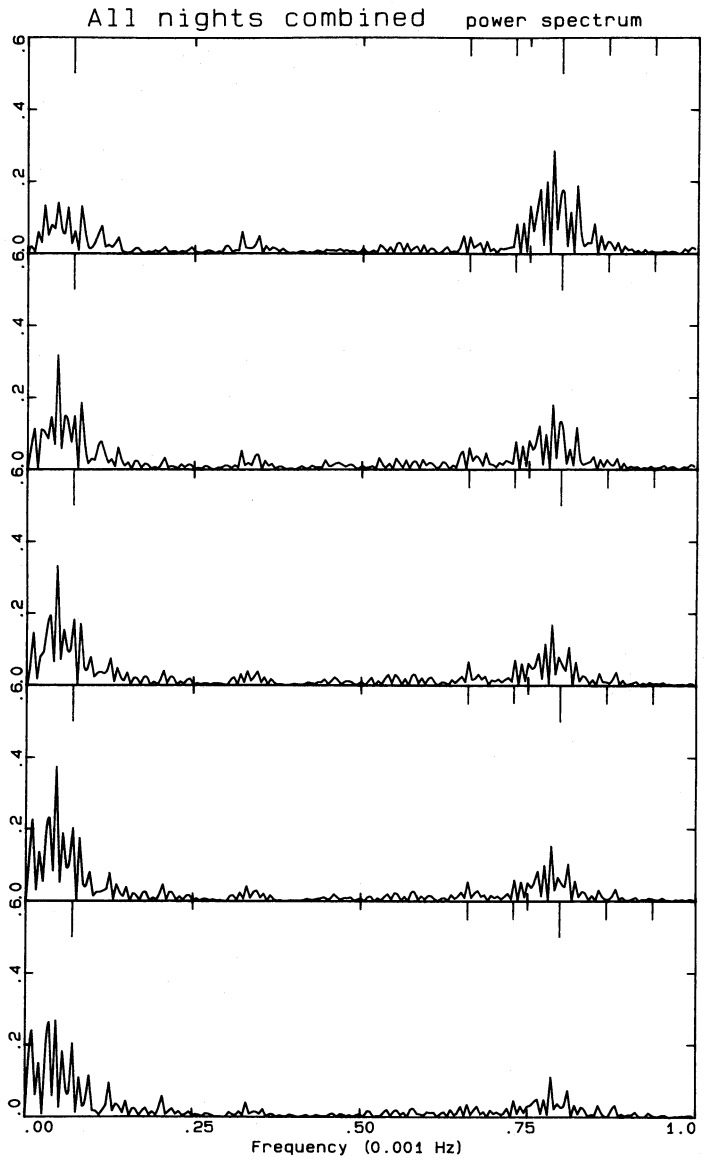

FIG. 5b

orbital ephemeris, the values do not show relevant changes; the shape of the folded light curve is still not sinusoidal, although the deviations are of similar extent at all wavebands).

To complete the discussion initiated in § II*a*[ii] above about the relative phasing of the optical and X-ray light curves, we may now compare them directly (see Fig. 7). The optical light curve is sinusoidal, and is symmetric around phase 0. The 1983 X-ray light curve is more modulated, but well in phase with the optical one, while the 1985 one is rather different, less symmetric, with a deep minimum just before phase 0.

ii) *Spectroscopy*

A sequence of 91 spectra in the range 4020–5060 Å, with ~1.5 Å resolution (FWHM), were obtained during the night 1984 July 25–26 with the Royal Greenwich Observatory (RGO) spectrograph and the image photon counting system (IPCS) at the Isaac Newton Telescope (INT) at the Observatorio del Roque de los Muchachos in La Palma. The typical integration time for each spectrum was 100 s.

Frequent Cu-Ar arc observations were made, resulting in wavelength calibration accurate and stable to ~0.1 Å. A problem associated with the IPCS (and unknown at the time of our observations) occasionally caused the count rates to drop in a wavelength-dependent manner, which unfortunately has made our spectra photometrically unreliable.

The optical spectrum of H2215−086 (the average raw count spectrum is shown in Fig. 8) is characterized by a number of emission lines over a well-defined continuum; most notable are the Balmer lines Hβ, Hγ, and Hδ and the line He II λ4686, and with reduced intensity also the He I lines $\lambda\lambda$4026, 4471, 4921, and 5015, He II λ4542, and the CNO band at 4640–4660 Å. We have analyzed the H Balmer and He II λ4686 lines (only the latter and Hβ are shown in the figures).

The line profiles are extremely variable. A qualitative look can be obtained from Figure 9, which shows the line profiles averaged over the total observing period, as well as over 10 orbital phase intervals (each one 0.1 wide) using the SM ephemeris. One can see the following:

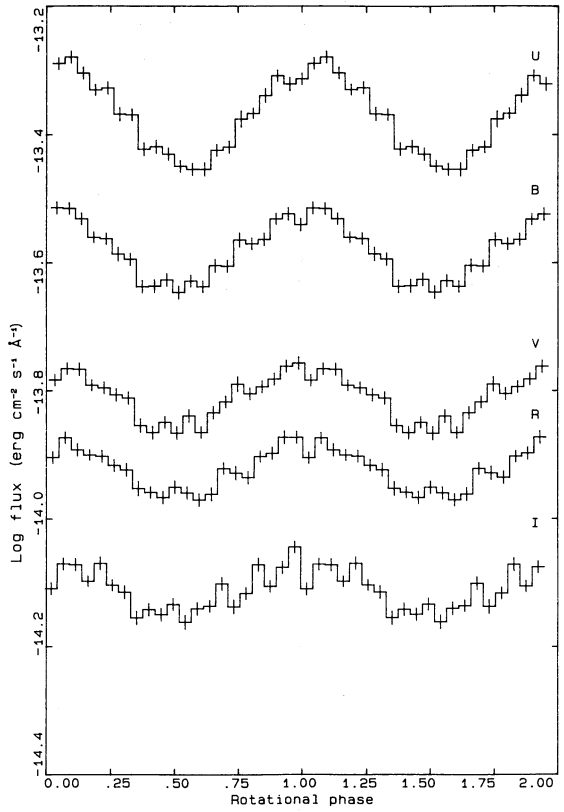

FIG. 6*a*

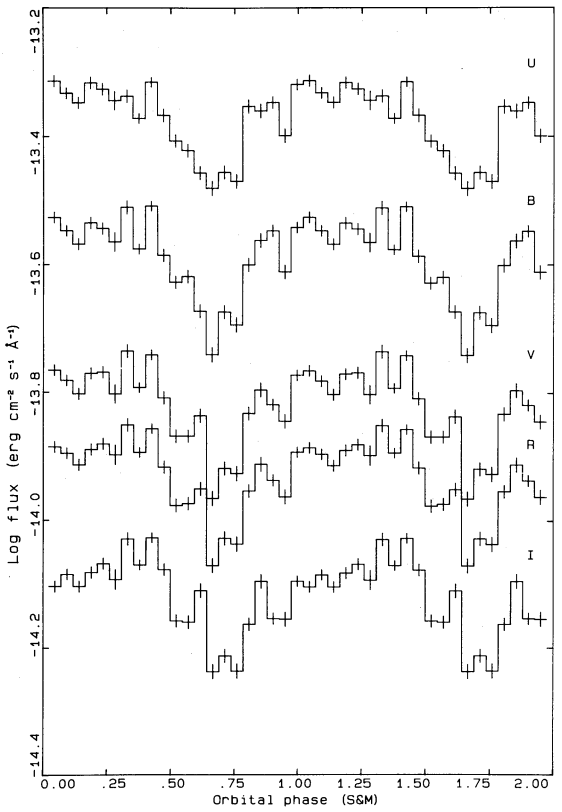

FIG. 6*b*

FIG. 6.—Folded optical light curves, (*a*) folded at the rotational period (according to SM) and (*b*) folded at the orbital period (according to SM). The five curves correspond, from top to bottom, to the *U*, *B*, *V*, *R*, and *I* bands.

1. All H lines show a complex profile with at least two components. The intensity of the blue component is generally lower than that of the red one. The two components are clearly distinct in the phase interval 0.5–0.8, then merge in a broad complex up to phase 1.3, when the blue component emerges again as a wide tail.

2. The He II line has a sharp and symmetric profile at phases 0.5 and 1.0, while a blue hump is apparent in the 0.5–1.0 interval, and a red wing in the 0.0–0.5 one.

3. The smallest FWHM of all lines occurs at orbital phase 1.0.

The equivalent widths and the radial velocities of He II λ4686 and of the main hydrogen lines as a function of time are reported in Figure 10, together with the periodograms. Given the difficulty of finding a multicomponent solution valid at all phases, velocities have been estimated by fitting the lines with a *single* Gaussian profile and taking the line centers. The main results are listed here (for the significances of the individual periodicities see Table 3B).

A strong peak at low frequencies, close to half of P_{orb}, is visible in the periodogram for all equivalent widths, and also at a similar period for the radial velocities of the hydrogen lines, while the radial velocity of the He II line shows a peak close to the orbital period. In both cases the large width of the peaks does not allow us to decide between the SM and our (§ II*b*[i]) photometric ephemeris.

A cluster of features at P_{rot} and at the surrounding sidebands S^- and S^+ is present in the periodograms for all equivalent widths. However, the strongest peak of the three is always the one at the sideband S^-, while the one at P_{rot} is marginal.

With respect to radial velocities, He II also behaves differently from the hydrogen lines. The latter show a notable peak at the sideband S^-, some minor evidence of S^+, and absolutely no trace of P_{rot}, while He II shows essentially the rotational frequency, with some evidence of S^-.

The presence of a rapid periodicity at P_{rot} or at the S^- sideband, indicated in the periodograms, can be confirmed by folding the data at the appropriate period. Modulation with amplitude ~ 50 km s^{-1} is apparent for He II at the rotational period (see Fig. 7 for relative phasing), while for Hβ the modulation occurs, with similar amplitude, at the S^- sideband frequency.

In order to single out the orbital modulation, we have averaged the individual measurements over each rotational cycle (according to the SM ephemeris).

The result for the He II radial velocity is shown in Figure 11. A sinusoidal variation is very clear, and a fit gives a period of 14,820 s, a systemic velocity of -62 km s^{-1}, an amplitude of 92 km s^{-1}, and the spectroscopic superior conjunction (zero crossing from positive to negative velocity) occurs around SM phase 0, but around phase 0.5 with the new ephemeris (compare the fiducial marks in Fig. 11.) This is in contrast to the statement by SM that the *inferior* conjunction corresponds to optical *minimum*. Note, however, that the time of minimum we predict from our ephemeris (we are unable to measure one directly, owing to the poor quality of the photometric data on

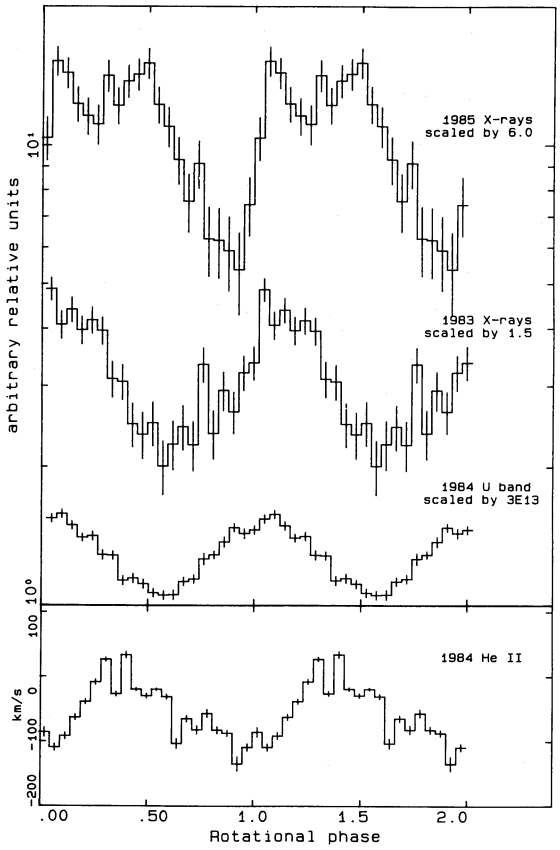

FIG. 7.—Relative phasing of X-ray and optical rotational modulation. The 1–10 keV light curves of 1983 and 1985, and the *U*-band light curve of 1984, are shown folded at the rotational period on a similar logarithmic scale to allow comparison in phase and amplitude. Also, the He II radial velocity is shown folded at the same period on a linear scale to allow comparison in phase.

July 26) falls close to inferior conjunction. However, we find it impossible to fit the 4.85 hr period to our spectroscopic data.

The case for radial velocity modulation for the hydrogen lines is less clear, since the data are more sparse even after averaging. No fitting of a period is possible; however, some indications may be obtained by fixing the period at the SM value. The systemic velocity is always positive (about 50 km s^{-1} for Hβ and Hγ, 130 km s^{-1} for Hδ); the largest amplitude is some 22 km s^{-1} for Hβ, and the modulation is approximately in phase with the He II line.

The orbital modulation of the equivalent widths of the He and H lines, averaged over the rotational cycle, is shown in Figure 11. Within one orbital cycle the equivalent width shows two equal maxima at phases (SM) 0.20 and 0.60, and a deep minimum at phase 0.45. A secondary minimum is apparent around phase 0.9; this is less shallow than the primary minimum for the hydrogen lines, while it is comparable for the He II line.

A fit with a sinusoid indicates a modulation at a periodicity close to half of P_{orb}, with all lines in phase, namely, at 7830 s with a mean of 12 Å and an amplitude of 1.6 Å for the He II, at 7950 s with a mean of 13 Å and an amplitude of 4.8 Å and Hβ, and at 7294 s with a mean of 9 Å and an amplitude of 2.3 Å for Hγ.

c) *Ultraviolet*

In 1983 and 1985 a total of eight low-dispersion spectra were obtained in each run, while seven spectra were taken in the 1984 run, exposing alternately in the short-wavelength (1200–1900 Å) and long-wavelength (2000–3000 Å) cameras. All spectra taken in 1983 and 1985 (with the exception of the last one of 1983) were exposed for a multiple of the rotational period (21, 42, or 63 minutes) to average out any rotational modulation effect. Different exposure times were used in 1984 in an attempt to improve the signal-to-noise ratio.

IUE spectra have been reduced with the IHAP package developed at ESO and available in Milan, and with the Starlink package available in Naples. The line-by-line extracted

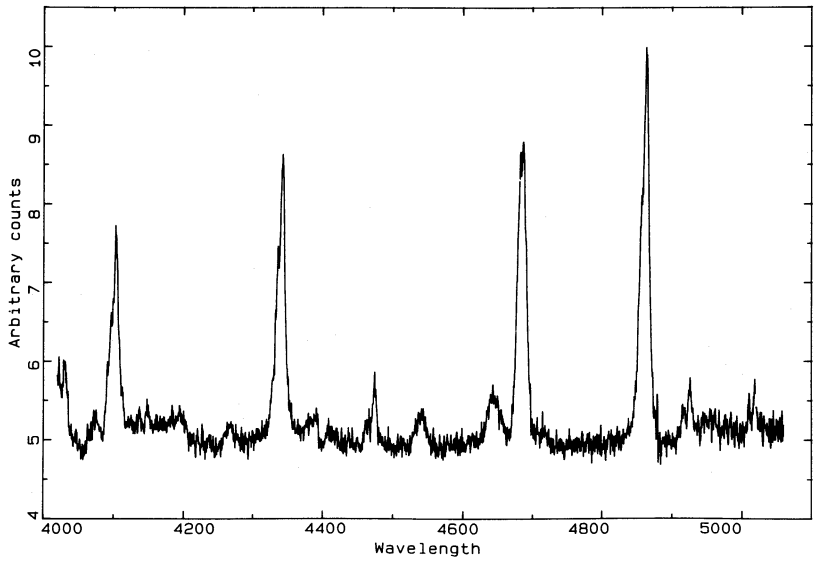

FIG. 8.—Average optical spectrum of H2215−086 (1984 July 26). The raw counts spectrum is reported, owing to problems with the IPCS calibrations (see text); therefore the slope of the continuum is not representative of the true energy distribution (see Fig. 13).

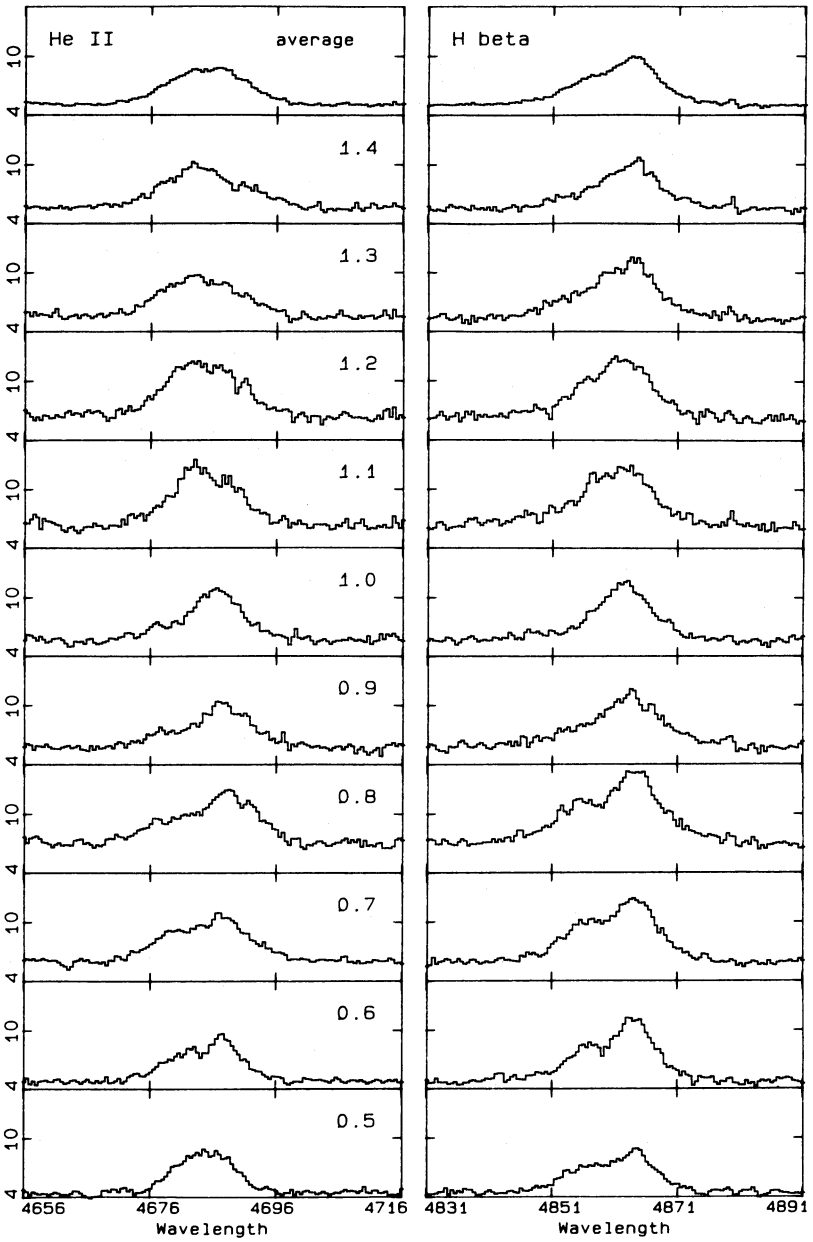

FIG. 9.—Profiles of the main spectral lines as a function of P_{orb}. The bottom 10 frames report the line profile averaged over intervals 0.1 wide in orbital phase (SM). The arrangement from bottom to top is in chronological order. The top frame reports the line profile averaged over the whole observing period.

spectra were carefully inspected for particle events, flaws, and presence of microphonic noise; particularly patchy background regions have also been removed. Calibration curves of Bohlin and Holm (1980) and Blades and Cassatella (1982) were used.

Average spectra in the 1200–3000 Å range are given in Figure 12 for 1983, 1984, and 1985. The state of 1984 appears higher than the others, and the 1985 one is somewhat higher than that of 1983, at variance with the X-ray behavior.

Emission lines typical of cataclysmic variables (N v λ1240, Si iv λ1400, C iv λ1550, He ii $\lambda\lambda$1640 and 2733, Mg ii λ2800, plus an occasional indication of N iv λ1718, N iii λ1750, C iii λ1175, and C ii λ1335) are present above a well-defined, flat continuum.

All SWP spectra show indication of a turnover shortward of 1400 Å (this feature has already been noticed by Szkody 1982). No dip at 2200 Å is apparent (see also Maraschi *et al.* 1984) either in the noisier SWP + LWP spectra or in the SWP + LWR archive spectra we have also examined. Therefore, no reddening correction was introduced.

Matching short-wavelength and long-wavelength spectra (taken at subsequent times) is generally not possible because of variability (see below). Each single spectrum was therefore fitted with a power law, and the resulting spectral indices are given in Table 6. The UV continuum energy distribution is essentially flat. This is remarkably different from the shape of the optical energy distribution (see Fig. 13).

A substantial variability in the continuum and lines is observed. Broad-band fluxes in selected line-free regions (reported in Table 6) show an erratic behavior (variation of a

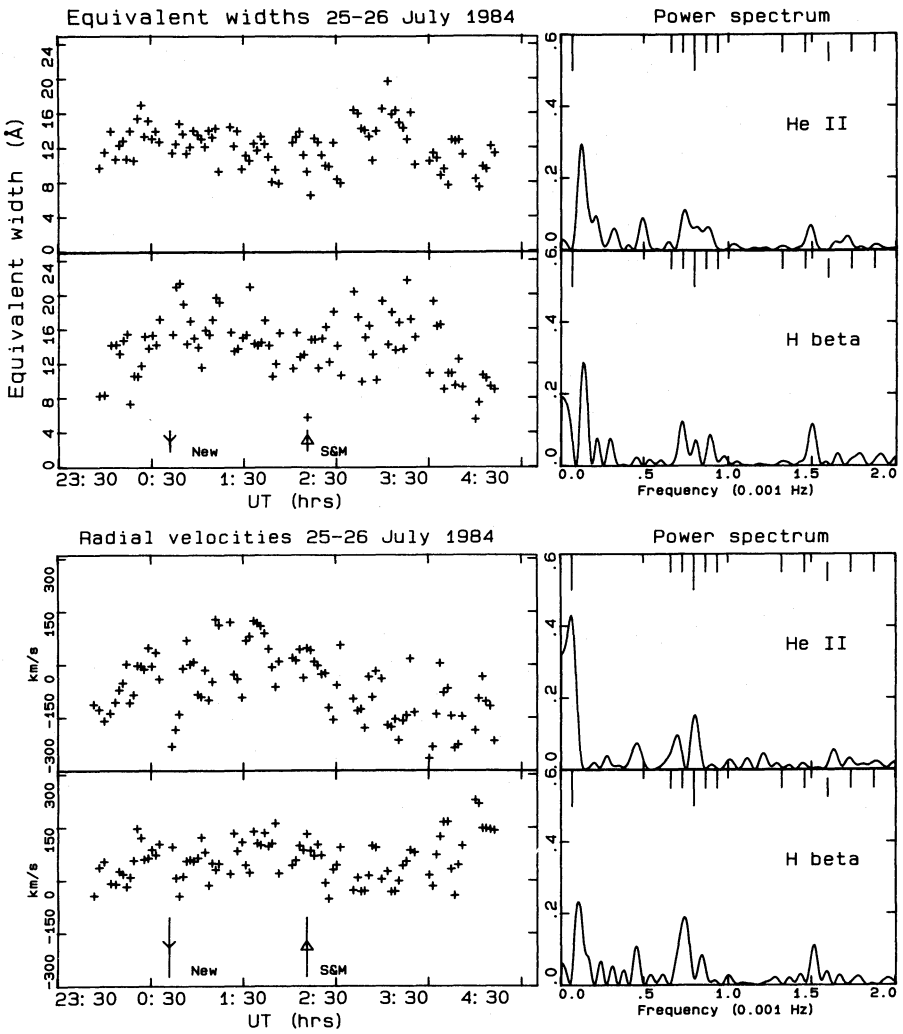

FIG. 10.—Time profiles of radial velocities and equivalent widths and related periodograms. The fiducial marks in the periodograms indicate the positions of the orbital frequency, of the S^{--} and S^{-} sidebands, of the rotational frequency, of the S^{+} and S^{++} sidebands, and of the first harmonic of the rotational frequency and sidebands. In the light curves the times of orbital phase 0 (according to SM and to the ephemeris derived in this paper) are marked with the same symbols used in Fig. 1.

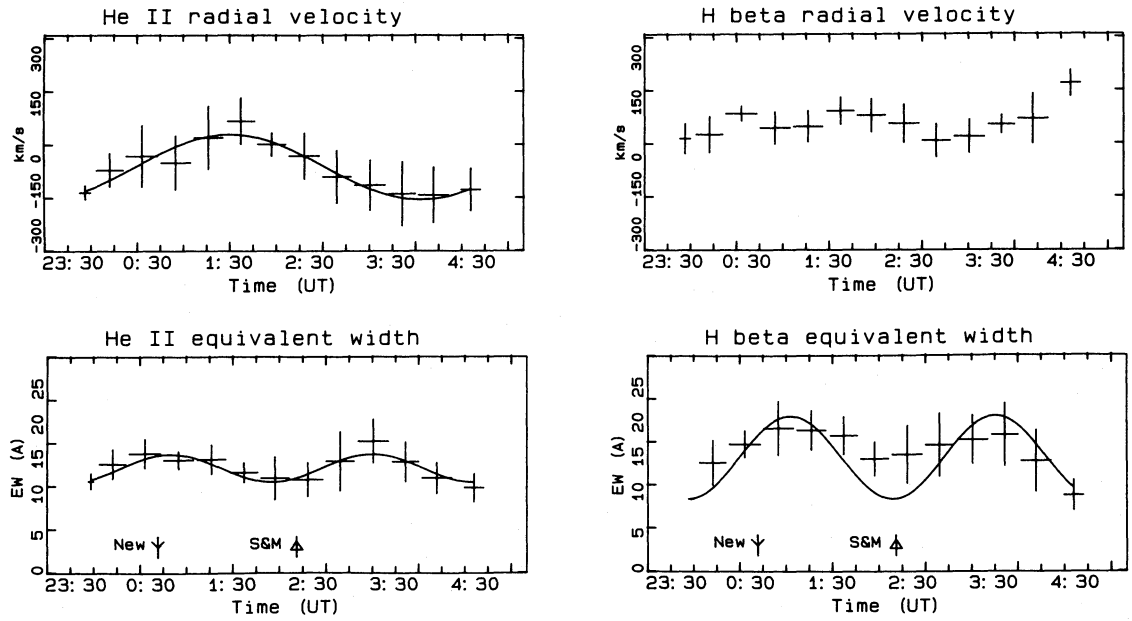

FIG. 11.—Sinusoidal fits to radial velocities. The result of sinusoidal fits at the orbital frequency to the radial velocity, and to the equivalent widths of He II and Hβ are reported. The data shown are averaged over entire rotational periods. The time of orbital phase 0 (according to SM and to the ephemeris derived in this paper) are marked with the same symbols used in Fig. 1.

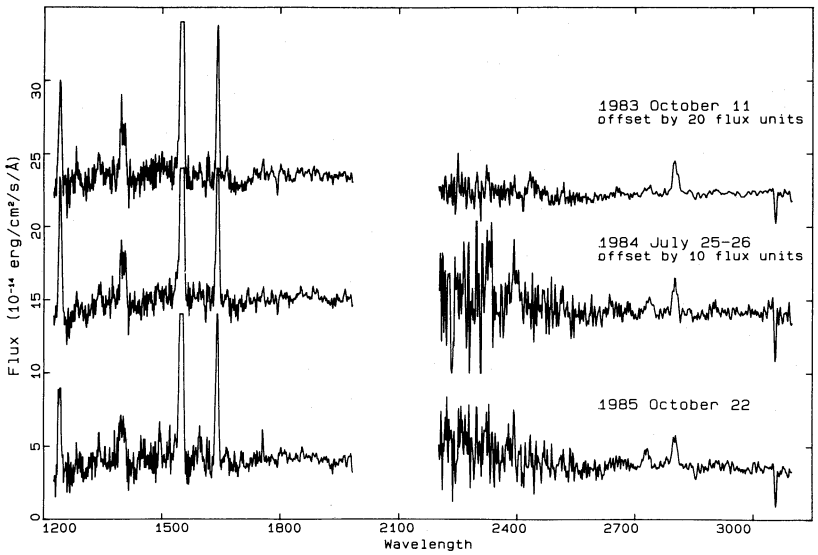

FIG. 12.—Average UV spectra for 1983, 1984, and 1985 observations

factor of 3, possibly secular, with 1984 being the highest state). Correlation of the continuum intensity with orbital phase was searched for (with both SM and our ephemeris): the short-wavelength fluxes have some hint of a minimum at phase 0 (only according to our ephemeris), but no other clear evidence was found (particularly in the long-wavelength range). We note that the colors (defined as F_{1475}/F_{1775} and F_{2425}/F_{2925}) are consistent within 10% and 20% respectively.

Line intensities and equivalent widths also show a large variability of a factor ~ 2. The line intensities appear to follow the same secular trend as the continuum. The equivalent widths of different lines (N V, C IV, and He II) give an indication of orbital modulation (minimum around phase 0) when the SM ephemeris is used. There is, however, no evidence at all of a double sine modulation (unlike the optical lines).

The line intensity ratios of N V, Si IV, C IV, and Mg II are

TABLE 6

SUMMARY OF ULTRAVIOLET MEASUREMENTS

IMAGE	ORBITAL PHASE		SW FLUX (1420–1520 Å)	LW FLUX (2500–2700 Å)	SPECTRAL FLUX
	SM	New			
			1983 October		
SWP 21272	0.49	0.99	3.32	...	−0.29 ± 0.03
SWP 21273	0.00	0.41	4.19	...	−0.39 ± 0.02
SWP 21274	0.43	0.77	2.87	...	−0.74 ± 0.04
SWP 21275	0.71	1.01	3.54	...	0.12 ± 0.02
LWR 16967.....	0.17	0.72	...	2.91	0.28 ± 0.04
LWP 2027	0.75	0.20	...	2.64	0.28 ± 0.03
LWP 2028	0.24	0.61	...	3.21	0.20 ± 0.06
LWP 2029	0.58	0.89	...	2.70	0.17 ± 0.07
			1984 July		
SWP 23511	0.59	0.14	5.89	...	0.13 ± 0.01
SWP 23512	0.94	0.43	4.98	...	0.10 ± 0.02
SWP 23513	0.29	0.72	4.10	...	−0.29 ± 0.08
LWP 3872	0.76	0.28	...	5.78	0.20 ± 0.04
LWP 3873	0.11	0.57	...	3.32	0.14 ± 0.01
LWP 3874	0.48	0.88	...	3.67	0.21 ± 0.01
			1985 October		
SWP 26965	0.40	0.93	3.22	...	0.00 ± 0.01
SWP 26966	0.72	0.20	5.00	...	0.16 ± 0.01
SWP 26967	0.05	0.47	5.44	...	0.09 ± 0.03
SWP 26968	0.50	0.83	3.22	...	−0.06 ± 0.03
LWP 6969	0.56	0.06	...	3.72	0.27 ± 0.03
LWP 6970	0.89	0.34	...	4.47	0.61 ± 0.06
LWP 6971	0.26	0.65	...	3.72	0.32 ± 0.06
LWP 6972	0.67	0.98	...	2.67	0.01 ± 0.01

NOTE.—The broad-band fluxes are in units of 10^{-14} ergs cm^{-2} s^{-1} Å^{-1}. The spectral indices α refer to a fit with a power law $F_\lambda \propto \lambda^{-\alpha}$; errors shown are 1 σ.

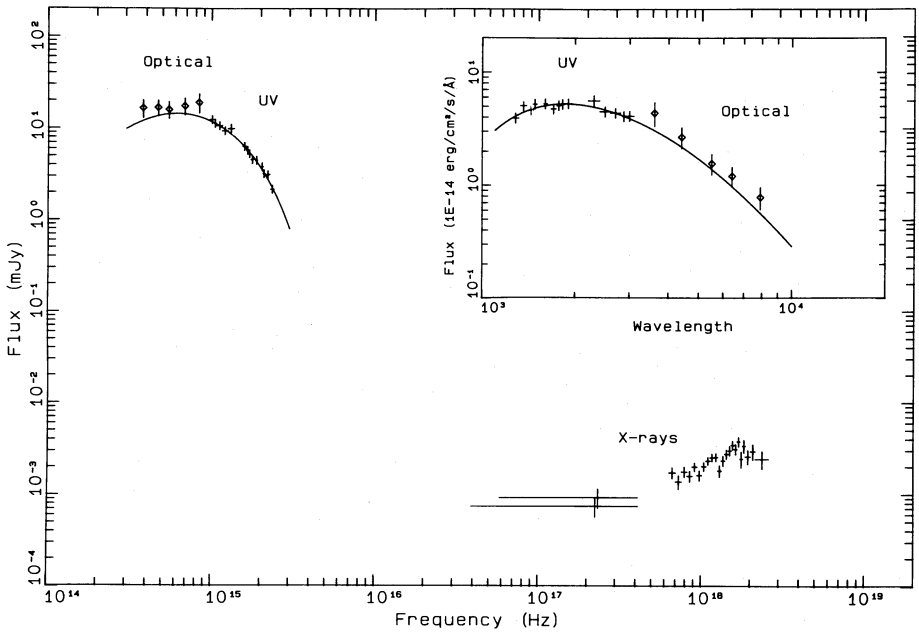

FIG. 13.—Composite spectrum of H2215−086. The UV average spectrum and the average quasi-simultaneous photometry of 1984 July 26 are shown together with the best-fit disk spectrum. The X-ray spectrum is the best-fit deconvolution of the 1983 high spectrum. The spectrum shown is at the source (the X-ray spectrum has been corrected for absorption, while such correction is negligible for the UV-optical spectrum [see text]).

quite consistent with the values expected for collisional excitation line formation at a temperature larger than 10^5 K. This appears to be a common feature in intermediate polars (Bonnet-Bidaud and Mouchet 1988). From the C IV and N V intensity ratio, by using the collisional excitation coefficients by Osterbrock (1974) and assuming the same temperature dependence for both lines, we derive a temperature of $(3.4 \pm 1.3) \times 10^5$ K.

The fact that the UV short-wavelength spectra generally show a slight negative slope (or no slope at all), while the long-wavelength ones have a slightly positive slope, suggests that the average UV continuum can be represented by a thick disk or a blackbody distribution. The two cases cannot be discriminated on the basis of the UV data alone.

A composite spectrum of H2215−086 (see Fig. 13) was made for the UV-optical range using the average 1984 UV spectrum in conjunction with the quasi-simultaneous *UBVRI* points (average values; we are aware this way that we are oversimplifying the energy distribution of the pulsed component). This composite spectrum was fitted with a thick-disk spectrum (Bath *et al.* 1974), obtaining $T_* = 39{,}300$ K (the 90% confidence range is 38,800–39,900 K), ratio of outer to inner radius $R_{out}/R_{in} = 11.5$ (10.3–13.5), and a flux in the 1000–10,000 Å interval of 1.81×10^{-10} ergs cm^{-2} s^{-1} (1.76–1.86); the best-fit spectrum is also shown in Figure 13.

A single blackbody (~14,000 K) does not give a good fit, falling short of the observed points both at short wavelengths and longward of the *V* band. Addition of a cooler (~3000 K) blackbody (as due to a possible companion, through as yet unobserved) may improve the fit in the red, but the discrepancy in the far-UV remains. A disk is hence apparently favored.

The actual energy distribution could be more complex than the simple disk model used above: compare the Williams and Ferguson (1982) model used by Szkody (1982). The fact that the *U* band point remains above the best fit could be due to the presence of a Balmer jump, as indicated in the optical spectrum reported by Szkody (1985), and in an unpublished spectrum by M. W. Pakull (1986, private communication), to which the matching of optical and UV spectra could be sensitive. It could therefore be useful to have simultaneous spectroscopy extending to the near-UV.

However, the simple disk fit already allows some estimate of the system parameters. Assuming an indicative distance of 500 pc (Patterson and Steiner 1983; Sherrington, Jameson, and Bailey 1984), the inner disk radius R_{in} is 2×10^9 cm, and the outer radius is $R_{out} = 2.3 \times 10^{10}$ cm. The latter comprises a substantial fraction of the typical Roche lobe size for a system of this kind, which, for a reasonable range of the mass ratio q (2–3.5), is $(4–5) \times 10^{10}$ cm. If, conversely, we assume that the disk is filling 90% of the Roche lobe, we get $R_{in} = 3.5 \times 10^9$ cm and a distance of 880 pc.

III. DISCUSSION

The overall average spectrum at the source (shown in Fig. 13) clearly consists of at least two components. The optical-UV component contains most of the observed luminosity. However, if the X-ray spectrum were to extend one more decade toward higher energies, the luminosities of the two components could be comparable.

As discussed in § IIc, the optical-UV component can be attributed to a disk extending from the Roche lobe to the Alfvén radius of a moderately magnetized white dwarf. According to the standard models for these systems, the X-rays should arise in a shock between the wide accretion column and the surface of the white dwarf, and should emit the bulk of the accretion luminosity (e.g., Lamb 1983). This can be reconciled with the observed energy distribution if, as mentioned above, the X-ray spectrum extends to higher energies, or if a substantial fraction of the X-ray emission is reprocessed into the UV-optical component. We note that the disk interpretation is based on *average* spectra, and neglects the fact that, as the optical pulsed fraction is substantial, the pulsed component is

likely to be a major contributor. Measurement of the amplitude and spectrum of the rotational modulation in the UV (which will be possible with the Hubble Space Telescope) will bring more light on this issue.

In the following we shall consider separately some implications of our results for the source model.

a) X-Ray Spectrum

Although the uncertainties in the spectral fits are rather large (see § II*a*[iii] and Table 5), there is a clear indication of variability with both the rotational phase and the epoch. The phase variability is dominated by a change in the column density, while some steepening has probably occurred in 1985 with respect to 1983. Absorption most probably occurs in the accretion column, which can easily account for depths of $\sim 10^{23}$ cm^{-2}. The variation of depth and orientation of the column can also be responsible for the modulation of the X-ray light curve.

All the observations (ME alone and ME + LE data) may be fitted by a photon spectral index ~ 0.6, which indicates a hard spectrum, even when compared with other members of the class (H2252−035: Pietsch *et al.* 1987; V1223 Sgr: Osborne *et al.* 1985*b*; GK Per: Watson, King, and Osborne 1985 and Norton, Watson, and King 1988; EX Hya: Rosen, Mason, and Córdova 1988; 3A 0729+103: McHardy *et al.* 1987), which are characterized by rather flat spectra. It is noticeable that thermal bremsstrahlung does not yield a satisfactory fit, contrary to expectation (simple shock models, e.g., Lamb 1983). The inadequacy of bremsstrahlung fits was also noted by McHardy *et al.* (1987) in the case of 3A 0729+103.

The hydrogen column derived by the LE + ME high phase of 1983 is compatible with zero, and incompatible with the value deduced in the high phase of 1985 on the basis of the ME data alone (which are, however, able to constrain the value only in a limited way). Therefore, an increase of the column density in 1985 is suggested, which may be associated with the change in the light curve. Alternatively, one can suppose that the LE flux is generated in a separate region with different absorption. In this regard we mention the suggestion by McHardy *et al.* (1987) of a second soft component being produced at the Alfvén radius in the case of 3A 0729+103.

b) X-Ray and Optical Spin Modulation

The short-period modulation is associated with the rotation of the white dwarf. The increase of the modulation of the X-ray light curve with decreasing energy, mentioned above, clearly indicates photoelectric absorption to be the modulation mechanism (compare Rosen, Mason, and Córdova 1988), rather than occultation of the accreting region by the body of the white dwarf (King and Shaviv 1984). If maximum absorption corresponds to the accretion column closest to the line of sight, as suggested by Warner (1985), the optical modulation can be understood as due to the heating of the accretion disk by the X-rays. Then the optical maximum corresponds to a phase when the accretion column is pointing away from the observer, and therefore the X-rays are at a maximum, since the absorption is at a minimum. For details on this kind of picture we refer to Figure 1 of Penning (1985). On the other hand, the similarity of the 1983 X-ray and 1984 optical light curves is puzzling in this model.

Difficulties for reprocessing of the continuum in the disk have been raised by Berriman *et al.* (1986), who agreed that this would lead to optically thin radiation, contrary to the observations. An alternative explanation of the spin modulation of the optical continuum is that it is due to cyclotron radiation at the shock region near the magnetic pole. The magnetic field strength is implied to be in excess of 10^6 G from the spin-down measurement (SM), which is compatible with this interpretation. However, an efficient mechanism of depolarization is required in order to explain the failure to detect any polarization to date (Berriman *et al.* 1986).

Our data confirm the spin modulation of the emission lines. Penning (1985) attributed this to reprocessing in the disk, following the work of Chanan, Nelson, and Morgan (1978) on DQ Her. In DQ Her, there is ample evidence that the spin-modulated components of both the continuum and the emission lines are due to reprocessing in the disk. In H2215−086 it is clear that the hydrogen Balmer and He II lines arise in different regions (this is demonstrated by their different modulation behavior). In particular, the phasing of the radial velocity modulation at the spin period argues against a disk origin for the emission lines. In fact, in the Chanan, Nelson, and Margon (1978) model for DQ Her, the phase of maximum redshift of the emission lines ($\phi_{\rm red}$) precedes pulse maximum by a quarter of a cycle. If we allow half a cycle uncertainty in the position of the pole (corresponding to absorption model and occultation model for the X-ray modulation), the value of $\phi_{\rm red}$ should be either 0.25 or 0.75. However, the observed $\phi_{\rm red}$ is around phase 0.5 (see Fig. 7). Our determination of $\phi_{\rm red}$ is not particularly precise, owing to the limited duration of our spectroscopic observation. Further spectroscopy would be useful in determining a tighter constraint on $\phi_{\rm red}$. The simplest assumption compatible with this measurement is to place the emission-line region in the accretion stream. This agrees with the absorption model for the X-ray modulation, which leads to $\phi_{\rm red} = 0.5$. This interpretation was also adopted for EX Hya by Hellier *et al.* (1987).

c) Orbital Modulation and Secular Variability

The detection of sidebands in the X-ray power spectra is rather interesting, since the only other object of the class for which sidebands have been observed in X-rays is H0542−407 (Tuohy *et al.* 1986). Sidebands in the optical power spectra are modeled by Warner (1985, 1986) as due to reprocessing of X-rays from the disk or the secondary. It is unclear whether a similar scenario can be extended to the reflection of X-rays.

A further important point is the discovery of a sideband at the frequency $\Omega_{\rm rot} + 2\Omega_{\rm orb}$, which was never detected before in intermediate polars, neither in the optical nor in the X-rays. Such a sideband would naturally arise if the white dwarf rotation were retrograde instead of prograde (with respect to the orbital motion). This possibility, however, was systematically rejected by Warner (1982, 1985, 1986) in his models of optical sidebands in intermediate polars. It should also be noted that the opposite periodicity at $\Omega_{\rm rot} - 2\Omega_{\rm orb}$ is detected in the optical.

Orbital modulations in the optical band (both photometric and spectroscopic) are consistent with a standard hot spot, an interaction region between the stream and the disk. The orbital modulation does not itself prove the presence of an accretion disk in H2215−086. However, the overall energy distribution argues in favor of this hypothesis.

Finally, we comment on the variation of the shape of the X-ray light curve between 1983 and 1985. The folded light curve of the 1983 observation is roughly sinusoidal, slightly

asymmetric with a sharp rise and a smoother decay. The 1985 folded light curve shows a double-peaked maximum with a pronounced dip (compare the case of V1223 Sgr; Osborne *et al.* 1985*b*). It is possible to attribute this variation to a secular variation in the shape of the accretion column. A similar variation of pulse shape was observed in only one of the other objects of the class: GK Per (Norton, Watson, and King 1988). The two pulse shapes observed in that case very closely resemble those of H2215−086. All other objects show pulses which are similar either to the 1983 type or to the 1985 type detected in H2215−086. This indicates that there are two favored configurations of the accretion column which repeat systematically and that transition between the two may be possible, even if not frequent.

The INT and JKT, on the island of La Palma, are operated by the Royal Greenwich Observatory at the Spanish Observatorio del Roque de los Muchachos of the Instituto de Astrofísica de Canarias. We thank our support astronomers Bob Fosbury and Derek Jones, and also V. Reyes, our night assistant. We also thank all operational and support staff of the *IUE* Observatory at VILSPA and the *EXOSAT* Observatory at ESOC, operated by ESA. We thank P. A. Charles for help in the arrangement of the optical observations, M. van der Klis for his participation in the same observations, and A. Smale and F. De Ponti for help in the data reduction. Finally, we would like to thank the anonymous referee for the careful reading of our manuscript and the numerous suggestions for style improvement.

REFERENCES

Bath, G. T., Evans, W. D., Papaloizou, J., and Pringle, J. E. 1974, *M.N.R.A.S.*, **190**, 447.
Berriman, G., Bailey, J., Axon, D. J., and Hough, J. H. 1986, *M.N.R.A.S.*, **223**, 469.
Bessell, M. S. 1979, *Pub. A.S.P.*, **91**, 589.
Blades, J. C., and Cassatella, A. C. 1982, *IUE ESA Newsletter*, **15**, 38.
Bohlin, J. D., and Holm, R. 1980, *IUE NASA Newsletter*, **10**, 37.
Bonnet-Bidaud, J. M., and Mouchet, M. 1988, in *Proc. Symposium on a Decade of UV Astronomy with the IUE Satellite* (Greenbelt), ed. E. J. Rolfe (ESA-SP 281), Vol. **1**, p. 271.
Chanan, G. A., Nelson, J. E., and Margon, B. 1978, B. 1978, *Ap. J.*, **226**, 963.
Chiappetti, L., *et al.* 1988, *Adv. Space Res.*, **8**, 309.
Cook, M. C., Watson, M. G., and McHardy, I. M. 1984, *M.N.R.A.S.*, **210**, 7P.
de Korte, P. A. J., Bleeker, J. A. M., and den Boggende, A. F. J. 1981, *Space Sci. Rev.*, **30**, 495.
Ferraz-Mello, S. 1981, *A.J.*, **86**, 619.
Hellier, C., Mason, K. O., Rosen, S. R., and Córdova, F. A. 1987, *M.N.R.A.S.*, **228**, 463.
King, A. R., and Shaviv, G. 1984, *M.N.R.A.S.*, **211**, 883.
Lamb, D. Q. 1983, in *IAU Colloquium 72, Cataclysmic Variables and Related Objects*, ed. M. Livio and G. Shaviv (Dordrecht: Reidel), p. 229.
Maraschi, L., *et al.* 1984, in *Proc. Fourth International Ultraviolet Explorer Conf.* (Rome), ed. R. Rolfe and B. Battrick (ESA SP-218), p. 427.
Marshall, F. E., Boldt, E. A., Holt, S. S., Mushotzky, R. F., Pravdo, S. H., Rothschild, R. E., and Serlemitsos, P. J. 1979, *Ap. J. Suppl.*, **40**, 657.
McHardy, I. M., Pye, J. P., Fairall, A. P., and Menzies, J. W. 1987, *M.N.R.A.S.*, **225**, 355.
Morrison, R., and McCammon, D. 1983, *Ap. J.*, **270**, 119.
Mouchet, M. 1983, *Messenger*, **34**, 3.
Mouchet, M., and Bonnet-Bidaud, J. M. 1984, in *Proc. Fourth International Ultraviolet Explorer Conf.* (Rome), ed. E. Rolfe and B. Battrick (ESA SP-218), p. 431.
Norton, A. J., Watson, M. G., and King, A. R. 1988, *M.N.R.A.S.*, **231**, 783.
Osborne, J. P., *et al.* 1985*a*, in *Proc. Internat. Symposium on X-Ray Astronomy* (Bologna), *X-Ray Astronomy '84*, ed. R. Giacconi and M. Oda, p. 63.
Osborne, J. P., Rosen, R., Mason, K. O., and Beuermann, K. 1985*b*, *Space Sci. Rev.*, **40**, 143.
Osterbrock, D. E. 1974, *Astrophysics of Gaseous Nebulae* (San Francisco: Freeman).
Pakull, M. W., and Beuermann, K. 1987, *Ap. Space Sci.*, **131**, 641.
Patterson, J., and Steiner, J. E. 1983, *Ap. J. (Letters)*, **264**, L61.
Penning, W. R. 1985, *Ap. J.*, **289**, 300.
Pietsch, W., Voges, W., Kendziorra, E., and Pakull, M. 1987, *Ap. Space. Sci.*, **130**, 281.
Rosen, S. R., Mason, K. O., and Córdova, F. A. 1988, *M.N.R.A.S.*, **231**, 549.
Shafter, A. W., and Macry, J. D. 1987, *M.N.R.A.S.*, **228**, 193 (SM).
Shafter, A. W., and Targan, D. M. 1982, *A.J.*, **87**, 655.
Sherrington. M. R., Jameson, R. F., and Bailey, J. 1984, *M.N.R.A.S.*, **210**, 1P.
Szkody, P. 1982, in *Proc. Symposium on Advances in UV Astronomy* (Greenbelt), *Four Years of UV Research*, ed. Y. Kondo, J. M. Mead, and R. D. Chapman (NASA CP-2238), p. 474.
———. 1985, in *Cataclysmic Variables and Low Mass X-Ray Binaries*, ed. D. Q. Lamb and J. Patterson (Dordrecht: Reidel), p. 385.
Tuohy, I. R., Buckley, D. A. H., Remillard, R. A., Bradt, H. V., and Schwartz, D. A. 1986, *Ap. J.*, **311**, 275.
Turner, M. J. L., and Smith, A. 1981, *Space Sci. Rev.*, **30**, 513.
Warner, B. 1983, in *Cataclysmic Variables and Related Objects*, ed. M. Livio and G. Shaviv (Dordrecht: Reidel), p. 155.
———. 1985, in *Cataclysmic Variables and Low-Mass X-Ray Binaries*, ed. D. Q. Lamb and J. Patterson (Dordrecht: Reidel), p. 269.
———. 1986, *M.N.R.A.S.*, **219**, 347.
Watson, M. G., King, A. R., and Osborne, J. 1985, *M.N.R.A.S.*, **212**, 917.
Williams, G. 1983, *Ap. J. Suppl.*, **53**, 523.
Williams, R. E., and Ferguson, D. H. 1982, *Ap. J.*, **257**, 672.

Note added in proof.—New photometric observations of FO Aqr, made after this paper was submitted, confirm that the orbital period is 4.85 hr and provide a refined ephemeris (J. P. Osborne and K. Mukai, *EXOSAT* Preprint No. 88 [1989]). The 4.85 hr period is supported also by a reanalysis of literature and unpublished observations by J. Patterson (*Inf. Bull. Var. Stars*, in press [1989]).

T. Belloni: Max-Planck-Institut für Extraterrestrische Physik, 8046 Garching bei München, Federal Republic of Germany

J.-M. Bonnet-Bidaud: Dph/SAP, CEN–Saclay, 91191 Gif-sur-Yvette, France

L. Chiappetti and E. G. Tanzi: Istituto di Fisica Cosmica e Tecnologie Relative del CNR, via Bassini 15, 20133 Milan, Italy

R. H. D. Corbet: Institute of Space and Astronautical Sciences, 3-1-1 Yoshinodai, Sagamihara, Kanagawa 229, Japan

C. Del Gratta: Istituto di Elettronica dello Stato Solido del CNR, via Cineto Romano 42, 00153 Rome, Italy

D. De Martino: Osservatorio Astronomico di Capodimonte, via Moiariello 16, 80131 Naples, Italy

L. Maraschi and A. Treves: Sezione di Astrofisica, Dipartimento di Fisica dell'Università, via Celoria 16, 20133 Milan, Italy

M. Mouchet: DAEC, Observatoire de Paris–Meudon, 5 Place J. Jannsen, 92195 Meudon, France

K. Mukai: Mullard Space Science Laboratory, University College London, Holmbury St. Mary, Dorking, Surrey RH5 6NT, United Kingdom

J. P. Osborne: Space Science Department of ESA, ESTEC, Postbus 299, 220 AG Noordwijk, The Netherlands